Chapter 2

SOME OCEAN MODEL FUNDAMENTALS

Stephen M. Griffies
NOAA/Geophysical Fluid Dynamics Laboratory, Princeton, New Jersey, USA

Abstract The purpose of these lectures is to present elements of the equations and algorithms used in numerical models of the large-scale ocean circulation. Such models generally integrate the ocean's *primitive equations*, which are based on Newton's Laws applied to a continuum fluid under hydrostatic balance in a spherical geometry, along with linear irreversible thermodynamics and subgrid scale (SGS) parameterizations. During formulations of both the kinematics and dynamics, we highlight issues related to the use of a generalized vertical coordinate. The vertical coordinate is arguably the most critical element determining how a model is designed and applications to which a model is of use.

Keywords: Ocean modelling, parameterization, vertical coordinate.

1. Concepts, themes, and questions

Numerical ocean models are computational tools used to understand and predict aspects of the ocean. They are a repository for our best ocean theories, and they provide an essential means to probe a mathematical representation of this very rich and complex geophysical system. That is, models provide an experimental apparatus for the scientific rationalization of ocean phenomena. Indeed, during the past decade, large-scale models have become *the* experimental tool of choice for many oceanographers and climate scientists. The reason for this state of affairs is largely due to improved understanding of both the ocean and ocean models, as well as increased computer power allowing for increasingly realistic representations of ocean fluid dynamics. Without computer models, our ability to develop a robust and testable intellectual basis for ocean and climate dynamics would be severely handicapped.

The remainder of this section introduces some basic concepts, themes, and questions, some of which are revisited later in the lectures. We present some philosophical notions which motivate a focus on fundamental concepts and notions when designing, constructing, and analyzing ocean models.

1.1 Model environments

The field of ocean model design is presently undergoing a rapid growth phase. It is arguable that the field has reached *adolescence*, with further maturation likely taking another 10-20 years as we take the models to a new level of integrity and innovation. Many applications drive this evolution, such as studies of climate change, operational oceanography, and ultra-refined resolution process studies.

One goal of many developers is that the next decade of model evolution will lead to a reduction in code distinctions which presently hinder the ability of modelers to interchange algorithms, make it difficult to directly compare and reproduce simulations using different codes, and increase the burdens of model maintenance in a world of increasingly complex computational platforms and diverse applications. Notably, the distinctions will not be removed by all modelers using a common algorithm. Such is unreasonable and unwarranted since different scientific problems call for different algorithmic tools. Instead, distinctions may be removed by the development of new codes with general algorithmic structures flexible enough to encompass multiple vertical coordinates, different horizontal grids, various subgrid scale (SGS) parameterizations, and alternate numerical methods.

The word *environment* has recently been proposed to describe these highly flexible and general codes. As yet, no model environment exists to satisfy the needs and desires of most modelers. Yet some models are moving in this direction by providing the ability to choose more than one vertical coordinate. This is a critical first step due to the central importance of vertical coordinates. The present set of lectures formulates the fundamental equations using generalized vertical coordinates, and these equations form the basis for generalized vertical coordinate ocean models. Ideally, the advent of general model environments will allow scientists to use the same code, even though they may use different vertical coordinates, horizontal grids, numerical methods, etc.

Many of the ideas presented here are an outgrowth of research and development with the Modular Ocean Model of Griffies et al., 2004, as well as the MITgcm (Marshall et al., 1997, Adcroft and Campin, 2004). The MITgcm provides for a number of depth-based and pressure-based

vertical coordinates. Another approach, starting from an isopycnal layered model, has been taken by the Hybrid Coordinate Ocean Model (HYCOM) of Bleck, 2002. HYCOM is arguably the most mature of the generalized vertical coordinate models.

From an abstract perspective, it is a minor point that different modelers use the same code, since in principle all that matters should be the continuum equations which are discretized. This perspective has, unfortunately, not been realized in practice. Differences in fundamentals of the formulation and/or numerical methods often serve to make the simulations quite distinct, even when in principle they should be nearly identical. Details do matter, especially when considering long time scale climate studies where small differences have years to magnify.

An argument against merging model development efforts is that there is creative strength in diversity, and so there should remain many ocean codes. A middle ground is argued here, whereby we maintain the framework for independent creative work and innovation, yet little effort is wasted developing redundant software and/or trying to compare different model outputs using disparate conventions. To further emphasize this point, we stress that the problems of ocean climate and operational oceanography are vast and complex, thus requiring tremendous human and computational resources. This situation calls for merging certain efforts to optimize available resources. Furthermore, linking modelers together to use a reduced set of code environments does not squelch creativity nor does it lead to less diversity in algorithmic approaches. Instead, environments ideally can provide modelers with common starting points from which to investigate different methodologies, parameterizations, and the like.

The proposal for model environments is therefore analogous to use of a few spoken/written languages (e.g., english, french) to communicate and formulate arguments, or a few computer languages (e.g., Fortran, C++) to translate numerical equations into computer code. Focusing on a few ocean model environments, rather than many ocean models, can lead to enhanced collaboration by removing awkward and frustrating barriers that exist between the presently wide suite of model codes. Ultimately, such will (it is hoped!) lead to better and more reproducible simulations, thus facilitating the maturation of ocean modelling into a more robust and respectable scientific discipline.

1.2 Some fundamental questions

It is possible to categorize nearly every question about ocean modelling into three classes.

1 Questions of model fundamentals, such as questions raised in this section.

2 Questions of boundary fluxes/forcing, from either the surface air-sea, river-sea, and ice-sea interactions, or forcing from the solid earth boundary. The lectures in this volume from Bill Large touch upon many of the surface flux issues.

3 Questions of analysis, such as how to rationalize the simulation to enhance ones ability to understand, communicate, and conceptualize.

If we ask questions about physical, mathematical, or numerical aspects of an ocean model, then we ask questions about ocean model fundamentals. The subject deals with elements of computational fluid mechanics, geophysical fluid mechanics, oceanography (descriptive and dynamic), and statistical physics. Given the wide scope of the subject, even a monograph such as Griffies, 2004 can only provide partial coverage. We consider even less in these lectures. The hope is that the material will introduce the reader to methods and ideas serving as a foundation for further study.

For the remainder of this section, we summarize a few of the many fundamental questions that designers and users often ask about ocean models. Some of the questions are briefly answered, yet some remain unaswered because they remain part of present day research. It is notable that model users, especially students learning how to use a model, often assume that someone else (e.g., their adviser, the author of a research article, or the author of a book) has devoted a nontrivial level of thought to answering many of the following questions. This is, unfortunately, often an incorrect assumption. The field of ocean modelling is not mature, and there are nearly as many outstanding questions as there are model developers and users. Such hopefully will provide motivation to the student to learn some fundamentals in order to help the field evolve.

Perhaps the most basic question to ask about an ocean model concerns the continuum equations that the model aims to discretize.

- Should the model be based on the non-hydrostatic equations, as relevant for simulations at spatial scales less than 1km, or is the hydrostatic approximation sufficient? Global climate models have all used the hydrostatic approximation, although the model of Marshall et al., 1997 provides an option for using either. Perhaps in 10-20 years, computational power will be sufficient to allow fully non-hydrostatic global climate simulations. Will the simulations

change drastically at scales larger than 1km, or do the hydrostatic models parameterize non-hydrostatic processes sufficiently well for most applications at these scales? Note that the accuracy of the hydrostatic approximation scales as the squared flow aspect ratio (ratio of vertical to horizontal length scales). Atmospheric modelers believe their simulations will be far more realistic with an explicit representation of non-hydrostatic dynamics, such as convection and cloud boundary layer processes. In contrast, it remains unclear how necessary non-hydrostatic simulations are for global ocean climate. Perhaps it will require plenty of experience running non-hydrostatic global models before we have unambiguous answers.

- Should the kinematics be based on incompressible volume conserving fluid parcels, as commonly assumed for ocean models using the Boussinesq approximation, or should the more accurate mass conserving kinematics of the non-Boussinesq fluid be used, as commonly assumed for the more compressible atmosphere. Ocean model designers are moving away from the Boussinesq approximation since only a mass conserving fluid can directly represent sea level changes due to steric effects (see Section 3.4.3 of Griffies, 2004), and because it is simple to use mass conserving kinematics by exploiting the isomorphisms between depth and pressure discussed by DeSzoeke and Samelson, 2002, Marshall et al., 2003, and Losch et al., 2004.

- Can the upper ocean surface be fixed in time with a rigid lid, as proposed decades ago by Bryan, 1969 and used for many years, or should it be allowed to fluctuate with a more realistic free surface so to provide a means to pass fresh water across the ocean surface and to represent tidal fluctuations? Most models today employ a free surface in order to remove the often unacceptable restrictions of the rigid lid. Additionally, many free surface methods remove elliptic problems from hydrostatic models. The absence of elliptic problems from the free surface models greatly enhances their computational efficiency on parallel computers (Griffies et al., 2001).

- Should tracers, such as salt, be passed across the ocean surface via virtual tracer fluxes, as required for rigid lid models, or should the model employ real water fluxes thus allowing for a natural dilution and concentration of tracer upon precipitation and evaporation, respectively? As discussed more fully in Section 3.6, the advent of free surface methods allows for modelers to jettison the unphysical

virtual tracer methods of the rigid lid. Nonetheless, virtual tracer fluxes remain one of the unnecessary legacy approximations plaguing some modern ocean models using free surface methods. The potential problems with virtual tracer fluxes are enhanced as the time scales of the integration go to the decade to century climate scale.

- What is the desired manner to write the discrete momentum equation: advective, as commonly done in B-grid models, or vector invariant, as commonly in C-grid models? The answer to this question may be based more on subjective notions of elegance than clear numerical advantage.

- How accurate should the thermodynamics be, such as the equation of state and the model's "heat" tracer? The work of McDougall and collaborators provides some guidance on these questions (McDougall, 2003, McDougall et al., 2003, Jackett et al., 2004). How important is it to get these things accurate? The perspective taken here is that it is useful to be more accurate and flexible with present day ocean climate models, since the temperature and salinity range over which they are used is quite wide, thus making the older approximations less valid. Additionally, many of the more accurate approaches have been refined to reduce their costs, thus making their use nearly painless.

After deciding on a set of model equations, further questions arise concerning how to cast the continuum partial differential equations onto a finite grid. First, we ask questions about the vertical coordinates. Which one to use?

- Geopotential (z-coordinate): This coordinate is natural for Boussinesq or volume conserving kinematics and is most commonly used in present-day global ocean climate models.

- Pressure: This coordinate is natural for non-Boussinesq or mass conserving kinematics and is commonly used in atmospheric models. As mentioned earlier, the isomorphism between pressure and depth allow for a straightforward transformation of depth coordinates to pressure coordinates, thus removing the Boussinesq approximation from having any practical basis. We return to this point in Section 6.

- Terrain following *sigma* coordinates: This coordinate is commonly used for coastal and estuarine models, with some recent efforts aimed as using it for global modelling (Diansky et al., 2002).

- Potential density or *isopycnal* coordinates: This coordinate is commonly used for idealized adiabatic simulations, with increasing use for operational and global climate simulations, especially when combined with pressure coordinates for the upper ocean in a hybrid context.

- Generalized hybrid vertical coordinates: Models formulated for general vertical coordinates allow for different vertical coordinates depending on the model application and fluid regime. Models with this facility provide an area of focus for the next generation of ocean models.

What about the horizontal grid? Although horizontal grids do not greatly determine the manner that many physical processes are represented or parameterized, they greatly influence on the representation of the solid-earth boundary, and affect details of how numerical schemes are implemented.

- Should we cast the model variables on one of the traditional A through E grids of Arakawa and Lamb, 1977? Which one? The B and C grids are the most common in ocean and atmospheric modelling. Why? Section 3.2 of Griffies et al., 2000a provides some discussion of this question along with references.

- What about spectral methods commonly used in atmospheric models? Can they be used accurately and effectively within the complex geometry of an ocean basin? Haidvogel and Beckmann, 1999 present a summary of these methods with application to the ocean. Typically, spectral methods have not been useful in the horizontal with realistically complex land-sea boundaries, nor in the vertical with realistically sharp pycnoclines. The reason is that a spectral representation of such strong gradients in the ocean can lead to unacceptable Gibbs ripples and unphysically large levels of spurious convective mixing.

- Should the horizontal grid cells be arranged according to spherical coordinates, even when doing so introduces a pesky coordinate singularity at the North Pole? What about generalized orthogonal coordinates such as a bipolar Arctic coupled to a spherical region south of the Arctic (Figure 1)? Such grids are very common today in global modelling, and their use is straightforward in practice since they retain the regular rectangular logic assumed by spherical coordinate models. Or what about strongly curved grid lines that contour the coast, yet remain locally orthogonal? Haidvogel and

Beckmann, 1999 provide some discussion of these grids and their uses.

- What about nested regions of refined resolution where it is critical to explicitly resolve certain flow and/or boundary features? Blayo at this school (see also Blayo and Debreu, 1999) illustrates the potentials for this approach. Can it be successfully employed for long term global climate simulations? What about coastal impacts of climate change? These are important questions at the forefront of ocean climate and regional modelling.

- Can a non-rectangular mesh, such as a cubed sphere, be successfully used to replace all coordinate singularities with milder singularities that allow for both atmosphere and ocean models to jettison polar filtering?[1] The work of Marshall et al., 2003 provide a compelling case for this approach, whereby both the ocean and atmosphere use the same grid and same dynamical core. Figure 2 provides a schematic of a cubed-sphere tiling of the sphere.

- What about icosahedrons, or spherical geodesics as invented by Buckminster Fuller? These grids tile the sphere in a nearly isotropic manner. Work at Colorado State University by David Randall and collaborators has shown some promise for this approach in the atmosphere and ocean.

- What about finite element or triangular meshes popular in engineering, tidal, and coastal applications? These meshes more accurately represent the solid earth boundary. Or what about time dependent adaptive approaches, whereby the grid is refined according to the time dependent flow regimes? Both methods have traditionally failed to perform well for realistic ocean climate simulations due to problems representing stratified and rotating fluids. However, as reported in this volume by Jens Schröter, some important and promising advances have been made by researchers at the University of Reading and Imperial College, both in England, as well as the Alfred-Wegener Institute in Germany. Their efforts have taken strides in overcoming some of the fundamental problems. If this area of research and development is given time to come to fruition, then perhaps in 10 years we will see finite ele-

[1] Polar filtering is a method to reduce the spatial scales of the simulation as one approaches the coordinate singularity at the North Pole. Many computational and numerical problems have been encountered with this approach.

ments commonly used for regional and global models. Such could represent a major advance in ocean modelling.

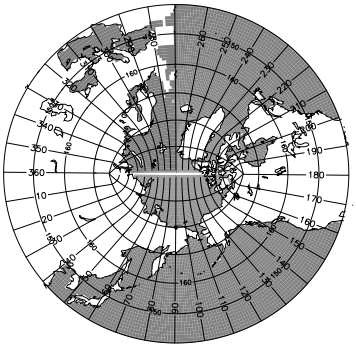

Figure 1. Illustration of the bipolar Arctic as prescribed by Murray, 1996 (see his Figure 7) and realized in the global model discussed in Griffies et al., 2005. A similar grid has also been proposed by Madec and Imbard, 1996. Shown here are grid lines which are labeled with the integers for the grid points. The grid has 360 points in the generalized longitude direction, and 200 points in the generalized latitude direction. This, or similar, bipolar Arctic grids are commonly used in global ocean modelling to overcome problems with the spherical coordinate singularity at the North Pole. Note that the cut across the Arctic is a limitation of the graphics, and does not represent a land-sea boundary in the model domain.

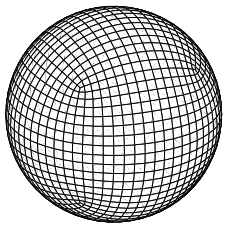

Figure 2. Cubed sphere tiling of the sphere. Note the singularities at the cube corners are much milder than a spherical coordinate singularity found with spherical grids at the poles. The cubed sphere tiling has been implemented in the MITgcm for both the atmosphere and ocean model components. This figure was kindly provided by Alistair Adcroft, a developer of the MITgcm.

What processes are represented explicitly, and what are the important ones to parameterize? This is one of the most critical and difficult questions of ocean model design and use. The lectures by Anne Marie Treguier from this school summarizes many of the issues. She notes that the choice of model resolution and parameterization prejudices the simulation so much so that they effectively determine the "ocean" to be simulated. Discussions in Chassignet and Verron, 1998 thoroughly survey various aspects of the parameterization problem. This book is from a 1998 school on ocean modelling and parameterization. Many of the issues raised there are still unresolved today. Finally, Griffies, 2004 has much to say about some of the common parameterizations used in ocean climate models.

Numerical methods are necessary to transform the continuum equations into accurate and efficient discrete equations for stepping the ocean forward in time. There are many methods of use for doing this task.

- Should they be based on finite volume methods? Such methods are becoming more common in ocean modelling. They provide the numericist with a useful means to take the continuum equations and cast them onto a finite grid.

- What sorts of time stepping schemes are appropriate, and what properties are essential to maintain? Will the ubiquitous leap-frog methods[2] be supplanted by methods that avoid the problematic time splitting mode? Chapter 12 of Griffies, 2004 provides a discussion of these points, and argues for the use of a time staggered method, similar to that discussed by Adcroft and Campin, 2004 and used in the Hallberg Isopycnal Model (Hallberg, 1997) and Modular Ocean Model version 4 (Griffies et al., 2004).

- Should the numerical equations maintain a discrete analog to conservation of energy, tracer, potential vorticity, and potential enstrophy satisfied by the ideal continuum equations? For long term climate simulations, tracer conservation is critical. What about the other conserved quantities?

- What are the essential features needed for the numerical tracer advection operator? Should it maintain positivity of the tracer field? Can such advection operators, which are nonlinear, be easily realized in their adjoint form as required for 4D variational

[2]As noted in Griffies et al., 2000a, the majority of ocean models supported for large-scale oceanography continue to use the leap-frog discretization of the time tendency.

assimilation (see the lectures at this school from Jens Schröter as well as Thuburn and Haine, 2001).

- How should the model treat the Coriolis force? On the B-grid, it is common to do so implicitly or semi-implicitly in time, but this method is not available on the C-grid since the velocity components are not coincident in space. Also, the C-grid spatial averaging of the Coriolis force can lead to problematical null modes (Adcroft et al., 1999).

- What about the pressure gradient calculation? We return to this question in Section 5, where comments are made regarding the difficulties of computing the pressure gradient.

1.3 Two themes

There are two themes emphasized in these lectures.

- How the vertical coordinate is treated is the most fundamental element of an ocean model design.

- The development of ocean model algorithms should be based on rational formulations starting from fundamental principles.

The first theme concerns the central importance of vertical coordinates in ocean model design. Their importance stems from the large distinctions at present between algorithms in models with differing vertical coordinates. Further differences arise in analysis techniques. These fundamental and pervasive distinctions have led to disparate research and development communities oriented around models of a particular class of vertical coordinate. One purpose of these lectures is to describe methods whereby these distinctions at the formulation stage are minimized, thus in principle facilitating the design of a single code capable of employing many vertical coordinates.

The second theme is a "motherhood" statement. What scientist or engineer would disagree? Nonetheless, it remains nontrivial to satisfy for three reasons. First, there are many important elements of the ocean that we do not understand. This ignorance hinders our ability to prescribe rational forms for the very important SGS operators. Second, some approximations (e.g., Boussinesq approximation, rigid lid approximation, virtual tracer fluxes), made years ago for good reasons then, often remain in use today yet need not be made with our present-day modelling capabilities and requirements. These *legacy approximations* often compromise a model's ability to realistically simulate certain aspects of the ocean and/or its interactions with other components of the

climate system. Third, developers are commonly under intense time pressures to "get the model running." These pressures often prompt *ad hoc* measures which, unfortunately, tend to stay around far longer than originally intended.

2. Kinematics of flow through a surface

In our presentation of ocean model fundamentals, we find it useful to start with a discussion of fluid kinematics. Kinematics is that area of mechanics concerned with the intrinsic properties of motion, independent of the dynamical laws governing the motion. In particular, we establish expressions for the transport of fluid through a specified surface. The specification of such transport arises in many areas of oceanography and ocean model design.

There are three surfaces of special interest in this section.

- The lower ocean surface which occurs at the time independent solid earth boundary. This surface is commonly assumed to be impenetrable to fluid.[3] The expression for fluid transport at the lower surface leads to the *solid earth kinematic boundary condition.*
- To formulate budgets for mass, tracer, and momentum in the ocean, we consider the upper ocean surface to be a time dependent permeable membrane through which precipitation, evaporation, ice melt, and river runoff pass. The expression for fluid transport at the upper surface leads to the *upper ocean kinematic boundary condition.*
- A surface of constant generalized vertical coordinate, s, is of importance when establishing the balances of mass, tracer, and momentum within a layer of fluid whose upper and lower bounds are determined by surfaces of constant s. Fluid transport through this surface is said to constitute the *dia-surface* transport.

2.1 Infinitesimal fluid parcels

Mass conservation for an infinitesimal parcel of fluid means that as it moves through the fluid, its mass is constant in time

$$\frac{\mathrm{d}M}{\mathrm{d}t} = 0. \tag{1}$$

[3]This assumption may be broken in some cases. For example, when the lower boundary is a moving sedimentary layer in a coastal estuary, or when there is seeping ground water. We do not consider such cases here.

In this equation, $M = \rho \, dV$ is the parcel's mass, ρ is its *in situ* density, and dV is its infinitesimal volume. The time derivative is taken following the parcel, and is known as a *material* or *Lagrangian* time derivative. Writing $dV = dx \, dy \, dz$, and defining the parcel's velocity as $\mathbf{v} = d\mathbf{x}/dt = (\mathbf{u}, w)$ leads to

$$\frac{d \ln \rho}{dt} = -\nabla \cdot \mathbf{v}. \tag{2}$$

Note that the horizontal coordinates $\mathbf{x}_h = (x, y)$ can generally be spherical coordinates (λ, ϕ), or any other generalized horizontal coordinate appropriate for the sphere, such as those illustrated in Figures 1 and 2 (see chapters 20 and 21 of Griffies, 2004 for a presentation of generalized horizontal coordinates).

For many purposes in fluid mechanics as well as ocean model design, it is useful to transform the frame of reference from the moving parcel to a fixed point in space. This transformation takes us from the material or Lagrangian frame to the *Eulerian* frame. It engenders a difference in how observers measure time changes in a fluid parcel's properties. In particular, the material time derivative picks up a *transport* or *advective* term associated with motion of the parcel

$$\boxed{\frac{d}{dt} = \partial_t + \mathbf{v} \cdot \nabla.} \tag{3}$$

This relation allows us to write the Lagrangian expression (2) for mass conservation in an Eulerian conservation form[4]

$$\rho_{,t} + \nabla \cdot (\rho \, \mathbf{v}) = 0. \tag{4}$$

Fluids that conserve mass are said to be *compressible* since the volume of a mass conserving fluid parcel can expand or contract based on pressure forces acting on the parcel, or properties such as temperature and salinity. However, in many circumstances, it is useful to consider the kinematics of a parcel that conserves its volume, in which case

$$\frac{1}{dV} \frac{dV}{dt} = -\nabla \cdot \mathbf{v} = 0. \tag{5}$$

The non-divergence condition $\nabla \cdot \mathbf{v} = 0$ provides a constraint on the parcel's velocity that must be satisfied at each point of the fluid. Fluid

[4]Throughout these lectures, a comma is used as a shorthand for partial derivative. Hence, $\rho_{,t} = \partial \rho / \partial t$. This notation follows Griffies, 2004, and is commonly used in mathematical physics. It is a useful means to distinguish a derivative from some of the many other uses of subscripts, such as a tensor component or as part of the name of a variable such as the fresh water flux q_w introduced in equation (27).

parcels that conserve their volume are known as *Boussinesq* parcels, whereas mass conserving parcels are *non-Boussinesq*. Non-Boussinesq parcels are generally considered in atmospheric dynamics, since the atmosphere is far more compressible than the ocean. However, most new ocean models are removing the Boussinesq approximation since straightforward means are known to solve the more general non-Boussinesq evolution using pressure-based coordinates.

2.2 Solid earth kinematic boundary condition

To begin our discussion of fluid flow through a surface, we start with the simplest surface: the time independent solid earth boundary. As mentioned earlier, one typically assumes in ocean modelling that there is no fluid crossing the solid earth lower boundary. In this case, a no-normal flow condition is imposed at the solid earth boundary at the depth

$$z = -H(x, y). \tag{6}$$

To develop a mathematical expression for the boundary condition, we note that the outward unit normal pointing from the ocean into the underlying rock is given by[5] (see Figure 3)

$$\hat{\mathbf{n}}_{\rm H} = -\frac{\nabla(z + H)}{|\nabla(z + H)|}. \tag{7}$$

Furthermore, we assume that the bottom topography can be represented as a continuous function $H(x, y)$ that does not possess "overturns." That is, we do not consider caves or overhangs in the bottom boundary where the topographic slope becomes infinite. Such would make it difficult to consider the slope of the bottom in our formulations. This limitation is common for ocean models.[6]

A no-normal flow condition on fluid flow at the ocean bottom implies

$$\mathbf{v} \cdot \hat{\mathbf{n}}_{\rm H} = 0 \qquad \text{at} \quad z = -H(x, y). \tag{8}$$

Expanding this constraint into its horizontal and vertical components leads to

$$\mathbf{u} \cdot \nabla H + w = 0 \qquad \text{at} \quad z = -H(x, y), \tag{9}$$

[5]The three dimensional gradient operator $\nabla = (\partial_x, \partial_y, \partial_z)$ reduces to the two dimensional horizontal operator $\nabla_z = (\partial_x, \partial_y, 0)$ when acting on functions that depend only on the horizontal directions. To reduce notation clutter, we do not expose the z subscript in cases where it is clear that the horizontal gradient is all that is relevant.

[6]For hydrostatic models, the solution algorithms rely on the ability to integrate vertically from the ocean bottom to the top, uninterrupted by rock in between. Non-hydrostatic models do not employ such algorithms, and so may in principle allow for arbitrary bottom topography, including overhangs.

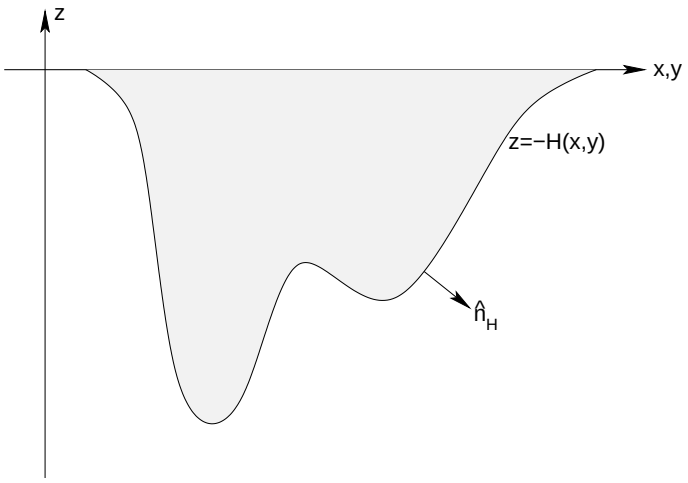

Figure 3. Schematic of the ocean's bottom surface with a smoothed undulating solid earth topography at $z = -H(x, y)$ and outward normal direction $\hat{\mathbf{n}}_{\mathrm{H}}$. Undulations of the bottom are far greater than the surface height (see Figure 4), as they can reach from the ocean bottom at 5000m-6000m to the surface over the course of a few kilometers (slopes on the order of 0.1 to 1.0). It is important for simulations to employ numerics that facilitate an accurate representation of the ocean bottom.

which can be written in the material derivative form

$$\frac{\mathrm{d}(z+H)}{\mathrm{d}t} = 0 \qquad \text{at} \quad z = -H(x,y). \tag{10}$$

Equation (10) expresses in a material or Lagrangian form the impenetrable nature of the solid earth lower surface, whereas equation (9) expresses the same constraint in an Eulerian form.

2.3 Generalized vertical coordinates

We now consider the form of the bottom kinematic boundary condition in generalized vertical coordinates. Generalized vertical coordinates provide the ocean theorist and modeler with a powerful set of tools to describe ocean flow, which in many situations is far more natural than the more traditional geopotential coordinates (x, y, z) that we have been using thus far. Therefore, it is important for the student to gain some exposure to the fundamentals of these coordinates, as they are ubiquitous in ocean modelling today.

Chapter 6 of Griffies, 2004 develops a calculus for generalized vertical coordinates. Some experience with these equations is useful to nurture an intuition for ocean modelling in generalized vertical coordinates.

Most notably, these coordinates, when used with the familiar horizontal coordinates (x, y), form a non-orthogonal triad, and thus lead to some unfamiliar relationships. To proceed in this section, we present some salient results of the mathematics of generalized vertical coordinates, and reserve many of the derivations for Griffies, 2004.

When considering generalized vertical coordinates in oceanography, we always assume that the surfaces cannot overturn on themselves. This constraint means that the Jacobian of transformation between the generalized vertical coordinate

$$s = s(x, y, z, t) \tag{11}$$

and the geopotential coordinate z, must be one signed. That is, the specific thickness

$$\frac{\partial z}{\partial s} = z_{,s} \tag{12}$$

is of the same sign throughout the ocean fluid. The name *specific thickness* arises from the property that

$$\mathrm{d}z = z_{,s}\, \mathrm{d}s \tag{13}$$

is an expression for the thickness of an infinitesimal layer of fluid bounded by two constant s surfaces.

Deriving the bottom kinematic boundary condition in s-coordinates requires a relation between the vertical velocity component used in geopotential coordinates, $w = \mathrm{d}z/\mathrm{d}t$, and the pseudo-velocity component $\mathrm{d}s/\mathrm{d}t$. For this purpose, we refer to some results from Section 6.5.5 of Griffies, 2004. As in that discussion, we note isomorphic relations

$$\mathrm{d}z/\mathrm{d}t = z_{,t} + \mathbf{u} \cdot \nabla_s z + z_{,s}\, \mathrm{d}s/\mathrm{d}t \tag{14}$$

$$\mathrm{d}s/\mathrm{d}t = s_{,t} + \mathbf{u} \cdot \nabla_z s + s_{,z}\, \mathrm{d}z/\mathrm{d}t, \tag{15}$$

with rearrangement leading to

$$\mathrm{d}z/\mathrm{d}t = z_{,s}\, (\mathrm{d}/\mathrm{d}t - \partial_t - \mathbf{u} \cdot \nabla_z)\, s. \tag{16}$$

This expression is relevant when measurements are taken on surfaces of constant geopotential, or depth. To apply this relation to the ocean bottom, which is generally not a surface of constant depth, it is necessary to transform the constant depth gradient ∇_z to a horizontal gradient taken along the bottom. We thus proceed as in Section 6.5.3 of Griffies, 2004 and consider the time-independent coordinate transformation

$$(\overline{x}, \overline{y}, \overline{z}, \overline{t}) = (x, y, -H(x, y), t). \tag{17}$$

The horizontal gradient taken on constant depth surfaces, ∇_z, and the horizontal gradient along the bottom, $\nabla_{\overline{z}}$, are thus related by

$$\nabla_{\overline{z}} = \nabla_z - (\nabla H)\, \partial_z. \tag{18}$$

Using this result in equation (16) yields

$$s_{,z}\,(w + \mathbf{u}\cdot\nabla H) = (\mathrm{d}/\mathrm{d}t - \partial_t - \mathbf{u}\cdot\nabla_{\overline{z}})\, s \qquad \text{at} \quad z = -H. \tag{19}$$

The left hand side vanishes due to the kinematic boundary condition (9), which then leads to

$$\mathrm{d}s/\mathrm{d}t = (\partial_t + \mathbf{u}\cdot\nabla_{\overline{z}})\, s \qquad \text{at} \quad s = s(x, y, z = -H(x, y), t). \tag{20}$$

The value of the generalized coordinate at the ocean bottom can be written in the shorthand form

$$s_{\mathrm{bot}}(x, y, t) = s(x, y, z = -H, t) \tag{21}$$

which leads to

$$\boxed{\frac{\mathrm{d}\,(s - s_{\mathrm{bot}})}{\mathrm{d}t} = 0 \qquad \text{at} \quad s = s_{\mathrm{bot}}.} \tag{22}$$

This relation is analogous to equation (10) appropriate to z-coordinates. Indeed, it is actually a basic statement of the impenetrable nature of the solid earth lower boundary, which is true regardless the vertical coordinates.

2.4 Upper surface kinematic condition

The upper ocean surface is penetrable and time dependent and full of breaking waves. Changes in ocean tracer concentration arise from precipitation, evaporation, river runoff,[7] and ice melt. These fluxes are critical agents in forcing the large scale ocean circulation via changes in ocean density and hence the water mass characteristics.

To describe the kinematics of water transport into the ocean, it is useful to introduce an effective transport through a smoothed ocean surface, where smoothing is performed via an ensemble average. We assume that this averaging leads to a surface absent overturns or breaking waves, thus

[7]River runoff generally enters the ocean at a nonzero depth rather than through the surface. Many global models, however, have traditionally inserted river runoff to the top model cell. Such can become problematic numerically and physically when the top grid cells are refined to levels common in coastal modelling. Hence, more applications are now considering the input of runoff throughout a nonzero depth.

facilitating a mathematical description analogous to the ocean bottom just considered. The vertical coordinate takes on the value

$$z = \eta(x, y, t) \tag{23}$$

at this idealized ocean surface.

We furthermore assume that density of the water crossing the ocean surface is $\rho_{\rm w}$, which is a function of the temperature, salinity, and pressure. Different water densities can be considered for precipitation, evaporation, runoff, and ice melt, but this level of detail is not warranted for present purposes. The mass transport crossing the ocean surface can be written

$$(\text{MASS/TIME}) \text{ THROUGH SURFACE} = \hat{\mathbf{n}}_\eta \cdot \hat{\mathbf{n}}_{\rm w} \, (P - E + R) \, \rho_{\rm w} \, \mathrm{d}A_\eta. \tag{24}$$

In this expression, $P > 0$ is the volume per time per area of precipitation entering the ocean, $E > 0$ is the evaporation leaving the ocean, and $R > 0$ is the river runoff and ice melt entering the ocean. The unit normal

$$\hat{\mathbf{n}}_\eta = \frac{\nabla \, (z - \eta)}{|\nabla \, (z - \eta)|} \tag{25}$$

points from the ocean surface at $z = \eta$ into the overlying atmosphere, whereas the unit normal $\hat{\mathbf{n}}_{\rm w}$ orients the flow of the water mass transported across the ocean surface (see Figure 4). Finally, the area element $\mathrm{d}A_\eta$ measures the infinitesimal area on the ocean surface $z = \eta$, and it is given by (see Section 20.13.2 of Griffies, 2004)

$$\mathrm{d}A_\eta = |\nabla(z - \eta)| \, \mathrm{d}x \, \mathrm{d}y. \tag{26}$$

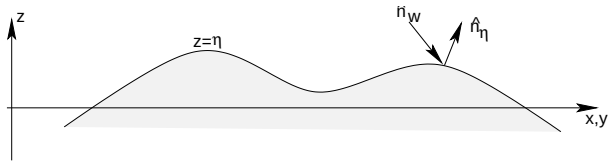

Figure 4. Schematic of the ocean's upper surface with a smoothed undulating surface height at $z = \eta(x, y, t)$, outward normal direction $\hat{\mathbf{n}}_\eta$, and freshwater normal direction $\hat{\mathbf{n}}_{\rm w}$. Undulations of the surface height are on the order of a few meters due to tidal fluctuations in the open ocean, and order 10m-20m in certain embayments (e.g., Bay of Fundy in Nova Scotia). When imposing the weight of sea ice onto the ocean surface, the surface height can depress even further, on the order of 5m-10m, with larger values possible in some cases. It is important for simulations to employ numerical schemes facilitating such wide surface height undulations.

We now introduce a more convenient expression for the mass transport across the surface by exploiting our assumption that the ocean surface has no overturns. For this purpose, define

$$q_{\rm w}\, {\rm d}A = \hat{\mathbf{n}}_\eta \cdot \hat{\mathbf{n}}_{\rm w}\, (P - E + R)\, {\rm d}A_\eta, \tag{27}$$

where

$${\rm d}A = {\rm d}x\, {\rm d}y \tag{28}$$

is the horizontal projection of the surface area element ${\rm d}A_\eta$. The volume per time per horizontal area of fluid crossing the ocean surface is therefore defined by $q_{\rm w}$

$$\boxed{\begin{aligned} q_{\rm w} &= \frac{\hat{\mathbf{n}}_\eta \cdot \hat{\mathbf{n}}_{\rm w}\, (P - E + R)\, {\rm d}A_\eta}{{\rm d}A} \\ &= \frac{(\text{VOLUME/TIME}) \text{ THROUGH FREE SURFACE}}{\text{HORIZONTAL AREA UNDER FREE SURFACE}}. \end{aligned}} \tag{29}$$

This is the surface water flux that appears in ocean model budgets for mass, tracer, and momentum.

As discussed in Section 3.4.3 of Griffies, 2004, the mass budget per horizontal area of a column of fluid extending from the ocean surface to its bottom is given by

$$\partial_t \left(\int_{-H}^{\eta} {\rm d}z\, \rho \right) = -\nabla \cdot \left(\int_{-H}^{\eta} {\rm d}z\, \rho\, \mathbf{u} \right) + q_{\rm w}\, \rho_{\rm w}. \tag{30}$$

This budget says that the time tendency of the total fluid mass per unit horizontal area within a column (left hand side) is balanced by the convergence of mass into the column (first term on the right hand side) and transport across the upper ocean surface (second term on the right hand side). To develop the upper ocean kinematic boundary condition, perform the derivatives in equation (30), keeping in mind Leibnitz's Rule when differentiating an integral. This step then leads to

$$[\rho\, (\partial_t + \mathbf{u} \cdot \nabla)\, \eta]_{z=\eta} + [\rho\, \nabla H \cdot \mathbf{u}]_{z=-H} + \int_{-H}^{\eta} {\rm d}z\, [\rho_{,t} + \nabla \cdot (\rho\, \mathbf{u})] = \rho_{\rm w}\, q_{\rm w}. \tag{31}$$

Use of the mass conservation equation (4) yields

$$[\rho\, (\eta_{,t} + \mathbf{u} \cdot \nabla \eta - w)]_{z=\eta} + [\rho\, (w + \nabla H \cdot \mathbf{u})]_{z=-H} = \rho_{\rm w}\, q_{\rm w}. \tag{32}$$

The solid earth kinematic boundary condition (9) allows us to cancel the second term on the left hand side, thus leading to the surface ocean

kinematic boundary condition

$$\rho\,(\partial_t + \mathbf{u}\cdot\nabla)\,\eta = \rho_{\rm w}\,q_{\rm w} + \rho\,w \qquad \text{at} \quad z = \eta \tag{33}$$

which can be written in the material form

$$\rho\left(\frac{\mathrm{d}(z-\eta)}{\mathrm{d}t}\right) = -\rho_{\rm w}\,q_{\rm w} \qquad \text{at} \quad z = \eta. \tag{34}$$

Contrary to the solid earth condition (10), where $z + H$ is materially constant, permeability of the ocean surface leads to a nontrivial material evolution of $z - \eta$.

To derive the analogous s-coordinate boundary condition, we proceed as for the bottom. Here, the coordinate transformation is time dependent

$$(\overline{x}, \overline{y}, \overline{z}, \overline{t}) = (x, y, \eta(x, y, t), t). \tag{35}$$

The horizontal gradient and time derivative operators are therefore related by

$$\nabla_{\overline{z}} = \nabla_z + (\nabla\,\eta)\,\partial_z \tag{36}$$

$$\partial_{\overline{t}} = \partial_t + \eta_{,t}\,\partial_z. \tag{37}$$

Hence, the relation (16) between vertical velocity components takes the following form at the ocean surface

$$w = z_{,s}\,(\mathrm{d}/\mathrm{d}t - \partial_{\overline{t}} - \mathbf{u}\cdot\nabla_{\overline{z}})\,s + (\partial_t + \mathbf{u}\cdot\nabla)\eta \qquad \text{at} \quad z = \eta. \tag{38}$$

Substitution of the z-coordinate kinematic boundary condition (33) leads to

$$\rho\,z_{,s}\;(\mathrm{d}/\mathrm{d}t - \partial_{\overline{t}} - \mathbf{u}\cdot\nabla_{\overline{z}})\;s = -\rho_{\rm w}\,q_{\rm w} \qquad \text{at} \quad s = s_{\rm top} \tag{39}$$

where $s_{\rm top} = s(x, y, z = \eta, t)$ is the value of the generalized vertical coordinate at the ocean surface. Reorganizing the result (39) leads to the material time derivative form

$$\boxed{\rho\,z_{,s}\left(\frac{\mathrm{d}(s - s_{\rm top})}{\mathrm{d}t}\right) = -\rho_{\rm w}\,q_{\rm w} \qquad \text{at} \quad s = s_{\rm top}} \tag{40}$$

which is analogous to the z-coordinate result (34). Indeed, it can be derived trivially by noting that $\mathrm{d}z/\mathrm{d}t = z_{,s}\,\mathrm{d}s/\mathrm{d}t$. Even so, it is useful to have gone through the previous manipulations in order to garner experience and confidence with the formalism. Such confidence becomes of particular use in the next section focusing on the dia-surface flux.

2.5 Dia-surface transport

We seek an expression for the flux of fluid passing through a surface of constant generalized vertical coordinate. The result will be an expression for the *dia-surface* transport. It plays a fundamental role in generalized vertical coordinate modelling. Our derivation here follows that given in Section 6.7 of Griffies, 2004.

At an arbitrary point on a surface of constant generalized vertical coordinate (see Figure 5), the flux of fluid in the direction normal to the surface is given by

$$\text{SEAWATER FLUX IN DIRECTION } \hat{\mathbf{n}} = \mathbf{v} \cdot \hat{\mathbf{n}}, \tag{41}$$

with

$$\hat{\mathbf{n}} = \nabla s \, |\nabla s|^{-1} \tag{42}$$

the surface unit normal direction. Introducing the material time derivative $\mathrm{d}s/\mathrm{d}t = s_{,t} + \mathbf{v} \cdot \nabla s$ leads to the equivalent expression

$$\mathbf{v} \cdot \hat{\mathbf{n}} = |\nabla s|^{-1} \, (\mathrm{d}/\mathrm{d}t - \partial_t) \, s. \tag{43}$$

That is, the normal component to a fluid parcel's velocity is proportional to the difference between the material time derivative of the surface and its partial time derivative.

Since the surface is generally moving, the net flux of seawater penetrating the surface is obtained by subtracting the velocity of the surface $\mathbf{v}^{(\mathrm{ref})}$ in the $\hat{\mathbf{n}}$ direction from the velocity component $\mathbf{v} \cdot \hat{\mathbf{n}}$ of the fluid parcels

$$\text{FLUX OF SEAWATER THROUGH SURFACE} = \hat{\mathbf{n}} \cdot (\mathbf{v} - \mathbf{v}^{(\mathrm{ref})}). \tag{44}$$

The velocity $\mathbf{v}^{(\mathrm{ref})}$ is the velocity of a reference point fixed on the surface, and it is written

$$\mathbf{v}^{(\mathrm{ref})} = \mathbf{u}^{(\mathrm{ref})} + w^{(\mathrm{ref})} \, \hat{\mathbf{z}}. \tag{45}$$

Since the reference point remains on the same $s = \text{const}$ surface, $\mathrm{d}s/\mathrm{d}t = 0$ for the reference point. Consequently, we can write the vertical velocity component $w^{(\mathrm{ref})}$ as

$$w^{(\mathrm{ref})} = -z_{,s} \, (\partial_t + \mathbf{u}^{(\mathrm{ref})} \cdot \nabla_z) \, s, \tag{46}$$

where equation (16) was used with $\mathrm{d}s/\mathrm{d}t = 0$. This result then leads to

$$\begin{aligned} \hat{\mathbf{n}} \cdot \mathbf{v}^{(\mathrm{ref})} &= \hat{\mathbf{n}} \cdot \mathbf{u}^{(\mathrm{ref})} + \hat{\mathbf{n}} \cdot \hat{\mathbf{z}} \, w^{(\mathrm{ref})} \\ &= -s_{,t} \, |\nabla s|^{-1}, \end{aligned} \tag{47}$$

which says that the normal component of the surface's velocity vanishes when the surface is static, as may be expected. It then leads to the following expression for the net flux of seawater crossing the surface

$$\boxed{\begin{aligned}\hat{\mathbf{n}} \cdot (\mathbf{v} - \mathbf{v}^{(\mathrm{ref})}) &= |\nabla s|^{-1} \, (\partial_t + \mathbf{v} \cdot \nabla) \, s \\ &= |\nabla s|^{-1} \, \mathrm{d}s/\mathrm{d}t.\end{aligned}} \tag{48}$$

Hence, the material time derivative of the generalized surface vanishes if and only if no water parcels cross it. This important result is used throughout ocean theory and modelling.

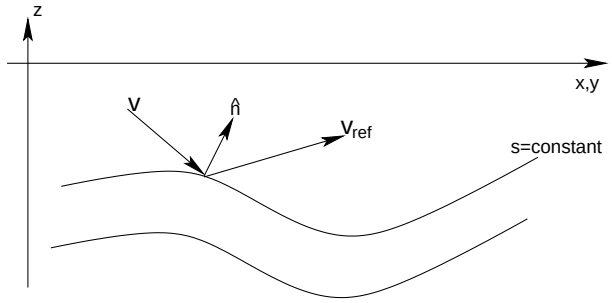

Figure 5. Surfaces of constant generalized vertical coordinate living interior to the ocean. An upward normal direction $\hat{\mathbf{n}}$ is indicated on one of the surfaces. Also shown is the orientation of a fluid parcel's velocity $\mathbf{v}$ and the velocity $\mathbf{v}^{(\mathrm{ref})}$ of a reference point living on the surface.

Expression (48) gives the volume of seawater crossing a generalized surface, per time, per area. The area normalizing the volume flux is that area $\mathrm{d}A_{(\hat{\mathbf{n}})}$ of an infinitesimal patch on the surface of constant generalized vertical coordinate with outward unit normal $\hat{\mathbf{n}}$. This area can be written (see equation (6.58) of Griffies, 2004)

$$\mathrm{d}A_{(\hat{\mathbf{n}})} = |z_{,s} \, \nabla s| \, \mathrm{d}x \, \mathrm{d}y. \tag{49}$$

Hence, the volume per time of fluid passing through the generalized surface is

$$\begin{aligned}(\text{VOLUME/TIME}) \text{ THROUGH SURFACE} &= \hat{\mathbf{n}} \cdot (\mathbf{v} - \mathbf{v}^{(\mathrm{ref})}) \, \mathrm{d}A_{(\hat{\mathbf{n}})} \\ &= |z_{,s}| \, (\mathrm{d}s/\mathrm{d}t) \, \mathrm{d}x \, \mathrm{d}y,\end{aligned} \tag{50}$$

and the magnitude of this flux is

$$|\hat{\mathbf{n}} \cdot (\mathbf{v} - \mathbf{v}^{(\mathrm{ref})}) \, \mathrm{d}A_{(\hat{\mathbf{n}})}| \equiv |w^{(s)}| \, \mathrm{d}x \, \mathrm{d}y. \tag{51}$$

We introduced the expression

$$w^{(s)} = z_{,s}\, \mathrm{d}s/\mathrm{d}t, \tag{52}$$

which measures the volume of fluid passing through the surface, per unit area $\mathrm{d}A = \mathrm{d}x\, \mathrm{d}y$ of the horizontal projection of the surface, per unit time. That is,

$$\boxed{\begin{aligned} w^{(s)} &\equiv \frac{\hat{\mathbf{n}} \cdot (\mathbf{v} - \mathbf{v}^{(\mathrm{ref})})\, \mathrm{d}A_{(\hat{\mathbf{n}})}}{\mathrm{d}A} \\ &= \frac{\text{(VOLUME/TIME) OF FLUID THROUGH SURFACE}}{\text{AREA OF HORIZONTAL PROJECTION OF SURFACE}}. \end{aligned}} \tag{53}$$

The quantity $w^{(s)}$ is called the dia-surface velocity component. It is directly analogous to the fresh water flux q_{w} defined in equation (27), which measures the volume of freshwater crossing the ocean surface, per unit time per horizontal area. To gain some experience with the dia-surface velocity component, it is useful to write it in the equivalent forms

$$\boxed{\begin{aligned} w^{(s)} &= z_{,s}\, \mathrm{d}s/\mathrm{d}t \\ &= z_{,s}\, \nabla s \cdot (\mathbf{v} - \mathbf{v}^{(\mathrm{ref})}) \\ &= (\hat{\mathbf{z}} - \mathbf{S}) \cdot (\mathbf{v} - \mathbf{v}^{(\mathrm{ref})}) \end{aligned}} \tag{54}$$

where

$$\begin{aligned} \mathbf{S} &= \nabla_s z \\ &= -z_{,s}\, \nabla_z s \end{aligned} \tag{55}$$

is the slope of the s surface as projected onto the horizontal directions. For example, if the slope vanishes, then the dia-surface velocity component measures the flux of fluid moving vertically relative to the motion of the generalized surface. When the surface is static and flat, then the dia-surface velocity component is simply the vertical velocity component $w = \mathrm{d}z/\mathrm{d}t$.

The expression (52) for $w^{(s)}$ allows one to write the material time derivative in one of the following equivalent manners

$$\boxed{\begin{aligned} \frac{\mathrm{d}}{\mathrm{d}t} &= \left(\frac{\partial}{\partial t}\right)_z + \mathbf{u} \cdot \nabla_z + w \left(\frac{\partial}{\partial z}\right) \\ &= \left(\frac{\partial}{\partial t}\right)_s + \mathbf{u} \cdot \nabla_s + \frac{\mathrm{d}s}{\mathrm{d}t} \left(\frac{\partial}{\partial s}\right) \\ &= \left(\frac{\partial}{\partial t}\right)_s + \mathbf{u} \cdot \nabla_s + w^{(s)} \left(\frac{\partial}{\partial z}\right), \end{aligned}} \tag{56}$$

where $\partial_s = z_{,s}\, \partial_z$. The last form motivates some to consider $w^{(s)}$ as a vertical velocity component that measures the rate at which fluid parcels penetrate the surface of constant generalized coordinate (see Appendix A to McDougall, 1995). One should be mindful, however, to distinguish $w^{(s)}$ from the generally different vertical velocity component $w = \mathrm{d}z/\mathrm{d}t$, which measures the water flux crossing constant geopotential surfaces.

We close with a few points of clarification for the case where no fluid parcels cross the generalized surface. Such occurs, in particular, in the case of adiabatic flows with $s = \rho$ an isopycnal coordinate. In this case, the material time derivative (56) only has a horizontal two-dimensional advective component $\mathbf{u} \cdot \nabla_s$. This result *should not* be interpreted to mean that the velocity of a fluid parcel is strictly horizontal. Indeed, it generally is not, as the previous derivation should make clear. Rather, it means that the transport of fluid properties occurs along surfaces of constant s, and such transport is measured by the convergence of horizontal advective fluxes as measured along surfaces of constant s. We revisit this point in Section 3.2 when discussing tracer transport (see in particular Figure 7).

3. Mass and tracer budgets

The purpose of this section is to extend the kinematics discussed in the previous section to the case of mass and tracer budgets for finite domains within the ocean fluid. In the formulation of ocean models, these domains are thought of as discrete model grid cells.

3.1 General formulation

Assume that mass and tracer are altered within a finite region by transport across boundaries of the region and by sources within the region. Hence, the tracer mass within an arbitrary fluid region evolves according to

$$\partial_t \left(\iiint C\, \rho\, \mathrm{d}V \right) = \iiint \mathcal{S}^{(\mathrm{C})}\, \rho\, \mathrm{d}V - \iint \mathrm{d}A_{(\hat{\mathbf{n}})}\, \hat{\mathbf{n}} \cdot [(\mathbf{v} - \mathbf{v}^{\mathrm{ref}})\, \rho\, C + \mathbf{J}]. \tag{57}$$

The left hand side of this equation is the time tendency for the tracer mass within the region, where C is the tracer concentration and ρ is the *in situ* fluid density (mass of seawater per volume). As discussed in Sections 5.1 and 5.6 of Griffies, 2004, C represents a mass of tracer per mass of seawater for non-thermodynamic tracers such as salt or biogeochemical tracers, whereas C represents the potential temperature or the conservative temperature (McDougall, 2003) for the "heat" tracer

used in the model. On the right hand side, $\mathcal{S}^{(C)}$ represents a tracer source with units of tracer concentration per time. As seen in Section 2.5, $\mathrm{d}A_{(\hat{\mathbf{n}})}\,\hat{\mathbf{n}}\cdot(\mathbf{v}-\mathbf{v}^{\mathrm{ref}})$ measures the volume per time of fluid penetrating the domain boundary at a point.

The tracer flux $\mathbf{J}$ arises from subgrid scale transport, such as diffusion and/or unresolved advection. This flux is assumed to vanish when the tracer concentration is uniform, in which case the tracer budget (57) reduces to a mass budget. In addition to the tracer flux, it is convenient to define the *tracer concentration flux* $\mathbf{F}$ via

$$\mathbf{J} = \rho\,\mathbf{F}, \tag{58}$$

where the dimensions of $\mathbf{F}$ are velocity $\times$ tracer concentration.

3.2 Budget for an interior grid cell

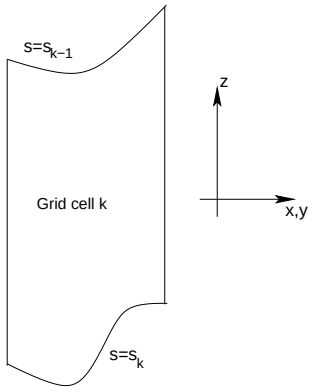

Figure 6. Schematic of an ocean grid cell labeled by the vertical integer k. Its sides are vertical and oriented according to $\hat{\mathbf{x}}$ and $\hat{\mathbf{y}}$, and its horizontal position is fixed in time. The top and bottom surfaces are determined by constant generalized vertical coordinates s_{k-1} and s_k, respectively. Furthermore, the top and bottom are assumed to always have an outward normal with a nonzero component in the vertical direction $\hat{\mathbf{z}}$. That is, the top and bottom are never vertical. Note that we take the convention that the discrete vertical label k increases as moving downward in the column, and grid cell k is bounded at its upper face by $s = s_{k-1}$ and lower face by $s = s_k$.

Consider the budget for a region bounded away from the ocean surface and bottom, such as that shown in Figure 6. There are two assumptions which define a grid cell region in this case.

- The sides of the cell are vertical, and so they are parallel to $\hat{\mathbf{z}}$ and aligned with the horizontal coordinate directions $(\hat{\mathbf{x}}, \hat{\mathbf{y}})$. Their horizontal positions are fixed in time.

- The top and bottom of the cell are defined by surfaces of constant generalized vertical coordinate $s = s(x, y, z, t)$. The generalized surfaces do not overturn, which means that $s_{,z}$ is single signed throughout the ocean.

These assumptions lead to the following results for the sides of the grid cell

$$\text{TRACER MASS ENTERING CELL WEST FACE} = \iint_{x=x_1} \mathrm{d}y\,\mathrm{d}z\,(u\,\rho\,C + \rho\,F^x) \tag{59}$$

$$\text{TRACER MASS LEAVING CELL EAST FACE} = -\iint_{x=x_2} \mathrm{d}y\,\mathrm{d}z\,(u\,\rho\,C + \rho\,F^x) \tag{60}$$

where $x_1 \leq x \leq x_2$ defines the domain boundaries for the east-west coordinates.[8] Similar results hold for the tracer mass crossing the cell in the north-south directions. At the top and bottom of the grid cell[9]

$$\text{TRACER MASS ENTERING CELL BOTTOM FACE} = \iint_{s=s_k} \mathrm{d}x\,\mathrm{d}y\;\rho\,(w^{(s)}\,C + F^{(s)}) \tag{61}$$

$$\text{TRACER MASS LEAVING CELL TOP FACE} = -\iint_{s=s_{k-1}} \mathrm{d}x\,\mathrm{d}y\;\rho\,(w^{(s)}\,C + F^{(s)}). \tag{62}$$

To reach this result, we used a result from Section 2.5 to write the volume flux passing through the top face of the grid cell

$$\mathrm{d}A_{(\hat{\mathbf{n}})}\,\hat{\mathbf{n}} \cdot (\mathbf{v} - \mathbf{v}^{\mathrm{ref}}) = w^{(s)}\,\mathrm{d}x\,\mathrm{d}y, \tag{63}$$

with $w^{(s)} = z_{,s}\,\mathrm{d}s/\mathrm{d}t$ the dia-surface velocity component. A similar relation holds for the bottom face of the cell. The form of the SGS flux passing across the top and bottom is correspondingly given by

$$\mathrm{d}A_{(\hat{\mathbf{n}})}\,\hat{\mathbf{n}} \cdot \mathbf{J} = J^{(s)}\,\mathrm{d}x\,\mathrm{d}y. \tag{64}$$

Since the model is using the generalized coordinate s for the vertical, it is convenient to do the vertical integrals over s instead of z. For this

[8] We use generalized horizontal coordinates, such as those discussed in Griffies, 2004. Hence, the directions east, west, north, and south may not correspond to the usual geographic directions. Nonetheless, this terminology is useful for establishing the budgets, whose validity is general.

[9] As seen in Section 6, for pressure-like vertical coordinates, s increases with depth. For depth-like vertical coordinates, s decreases with depth. It is important to keep this sign difference in mind when formulating the budgets in the various coordinates. Notably, the specific thickness $z_{,s}$ carries the sign.

purpose, recall that with $z_{,s}$ single signed, the vertical thickness of a grid cell is

$$\mathrm{d}z = z_{,s}\,\mathrm{d}s. \tag{65}$$

Bringing these results together, and taking the limit as the volume of the cell in (x, y, s) space goes to zero (i.e., $\mathrm{d}x\,\mathrm{d}y\,\mathrm{d}s \to 0$) leads to

$$\partial_t(z_{,s}\,\rho\,C) = z_{,s}\,\rho\,\mathcal{S}^{(\mathrm{C})} - \nabla_s\cdot[z_{,s}\,\rho\,(\mathbf{u}\,C+\mathbf{F})] - \partial_s\,[\,\rho\,(w^{(s)}\,C+F^{(s)})] \tag{66}$$

Notably, the horizontal gradient operator ∇_s is computed on surfaces of constant s, and so it is distinct generally from the horizontal gradient ∇_z taken on surfaces of constant z. Instead of taking the limit as $\mathrm{d}x\,\mathrm{d}y\,\mathrm{d}s \to 0$, it convenient for discretization purposes to take the limit as the time independent horizontal area $\mathrm{d}x\,\mathrm{d}y$ goes to zero, thus maintaining the time dependent thickness $\mathrm{d}z = z_{,s}\,\mathrm{d}s$ inside the derivative operators. In this case, the thickness weighted tracer mass budget takes the form

$$\boxed{\begin{aligned}\partial_t(\mathrm{d}z\,\rho\,C) = \mathrm{d}z\,\rho\,\mathcal{S}^{(\mathrm{C})} - \nabla_s\cdot[\mathrm{d}z\,\rho\,(\mathbf{u}\,C+\mathbf{F})] \\ - [\rho\,(w^{(s)}\,C+F^{(s)})]_{s=s_{k-1}} + [\rho\,(w^{(s)}\,C+F^{(s)})]_{s=s_k}.\end{aligned}} \tag{67}$$

Similarly, the thickness weighted mass budget is

$$\boxed{\begin{aligned}\partial_t(\mathrm{d}z\,\rho) = \mathrm{d}z\,\rho\,\mathcal{S}^{(\mathrm{M})} - \nabla_s\cdot(\mathrm{d}z\,\rho\,\mathbf{u}) \\ - (\rho\,w^{(s)})_{s=s_{k-1}} + (\rho\,w^{(s)})_{s=s_k}.\end{aligned}} \tag{68}$$

where $\mathcal{S}^{(\mathrm{M})}$ is a mass source with units of inverse time that is related to the tracer source via

$$\mathcal{S}^{(\mathrm{M})} = \mathcal{S}^{(\mathrm{C})}(C=1), \tag{69}$$

and the SGS flux vanishes with a uniform tracer

$$\mathbf{F}(C=1) = 0. \tag{70}$$

3.3 Budgets without dia-surface fluxes

To garner some experience with these budgets, it is useful to consider the special case of zero dia-surface transport, either via advection or SGS fluxes, and zero tracer/mass sources. In this case, the thickness weighted mass and tracer mass budgets take the simplified form

$$\partial_t(\mathrm{d}z\,\rho) = -\nabla_s\cdot(\mathrm{d}z\,\rho\,\mathbf{u}) \tag{71}$$

$$\partial_t(\mathrm{d}z\,\rho\,C) = -\nabla_s\cdot[\mathrm{d}z\,\rho\,(\mathbf{u}\,C+\mathbf{F})]. \tag{72}$$

The first equation says that the time tendency of the thickness weighted density (mass per area) at a point between two surfaces of constant

generalized vertical coordinate is given by the horizontal convergence of mass per area onto that point. The transport is quasi-two-dimensional in the sense that it is only a two-dimensional convergence that determines the evolution. The tracer equation has an analogous interpretation. We illustrate this situation in Figure 7. As emphasized in our discussion of the material time derivative (56), this simplification of the transport equation does not mean that fluid parcels are strictly horizontal. Indeed, such is distinctly not the case when the surfaces are moving.

A further simplification of the mass and tracer mass budgets ensues when considering adiabatic and Boussinesq flow in isopycnal coordinates. We consider ρ now to represent the constant potential density of the finitely thick fluid layer. In this case, the mass and tracer budgets reduce to

$$\partial_t(\mathrm{d}z) = -\nabla_\rho \cdot (\mathrm{d}z\,\mathbf{u}) \tag{73}$$

$$\partial_t(\mathrm{d}z\,C) = -\nabla_\rho \cdot [\mathrm{d}z\,(\mathbf{u}\,C + \mathbf{F})]. \tag{74}$$

Equation (73) provides a relation for the thickness of the density layers, and equation (74) is the analogous relation for the tracer within the layer. These expressions are commonly used in the construction of adiabatic isopycnal models, which are often used in the study of geophysical fluid mechanics of the ocean.

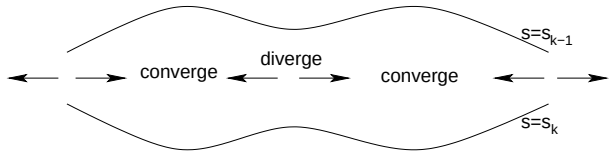

Figure 7. Schematic of the horizontal convergence of mass between two surfaces of constant generalized vertical coordinates. As indicated by equation (71), when there is zero dia-surface transport, it is just the horizontal convergence that determines the time evolution of mass between the layers. Evolution of thickness weighted tracer concentration in between the layers is likewise evolved just by the horizontal convergence of the thickness weighted advective and diffusive tracer fluxes (equation (72)). In this way, the transport is quasi-two-dimensional when the dia-surface transports vanish. A common example of this special system is an adiabatic ocean where the generalized surfaces are defined by isopycnals.

3.4 Cells adjacent to the ocean bottom

For a grid cell adjacent to the ocean bottom (Figure 8), we assume that just the bottom face of this cell abuts the solid earth boundary. The outward normal $\hat{\mathbf{n}}_{\mathrm{H}}$ to the bottom is given by equation (7), and the

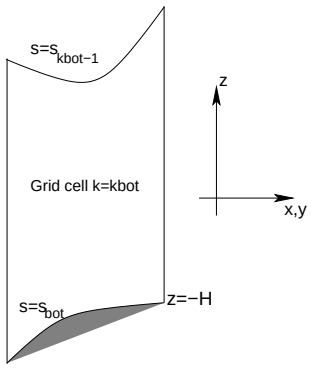

Figure 8. Schematic of an ocean grid cell next to the ocean bottom labeled by $k = k_{\rm bot}$. Its top face is a surface of constant generalized vertical coordinate $s = s_{\rm kbot-1}$, and the bottom face is determined by the ocean bottom topography at $z = -H$ where $s_{\rm bot}(x, y, t) = s(x, y, z = -H, t)$.

area element along the bottom is

$$\mathrm{d}A_{\rm H} = |\nabla(z + H)|\, \mathrm{d}x\, \mathrm{d}y. \tag{75}$$

Hence, the transport across the solid earth boundary is

$$-\iint \mathrm{d}A_{\rm H}\, \hat{\mathbf{n}}_{\rm H} \cdot (\mathbf{v}\, \rho\, C + \mathbf{J}) = \iint \mathrm{d}x\, \mathrm{d}y\, (\nabla H + \hat{\mathbf{z}}) \cdot (\mathbf{v}\, \rho\, C + \mathbf{J}). \tag{76}$$

We assume that there is zero mass flux across the bottom, in which case the advective flux drops out since $\mathbf{v} \cdot (\nabla H + \hat{\mathbf{z}}) = 0$ (equation (9)). However, the possibility of a nonzero geothermal tracer transport warrants a nonzero SGS tracer flux at the bottom, in which case the bottom tracer flux is written

$$Q^{(\rm C)}_{(\rm bot)} = (\nabla H + \hat{\mathbf{z}}) \cdot \mathbf{J}. \tag{77}$$

The corresponding thickness weighted budget is given by

$$\boxed{\begin{aligned} \partial_t\, (\mathrm{d}z\, \rho\, C) = {} & \mathrm{d}z\, \rho\, \mathcal{S}^{(\rm C)} - \nabla_s \cdot [\mathrm{d}z\, \rho\, (\mathbf{u}\, C + \mathbf{F})] \\ & - \Big[\rho\, (w^{(s)}\, C + z_{,s}\, \nabla s \cdot \mathbf{F})\Big]_{s=s_{kbot-1}} \\ & + Q^{(\rm C)}_{(\rm bot)}, \end{aligned}} \tag{78}$$

and the corresponding mass budget is

$$\boxed{\partial_t\, (\mathrm{d}z\, \rho) = \mathrm{d}z\, \rho\, \mathcal{S}^{(\rm M)} - \nabla_s \cdot (\mathrm{d}z\, \rho\, \mathbf{u}) - (\rho\, w^{s)})_{s=s_{kbot-1}}.} \tag{79}$$

3.5 Cells adjacent to the ocean surface

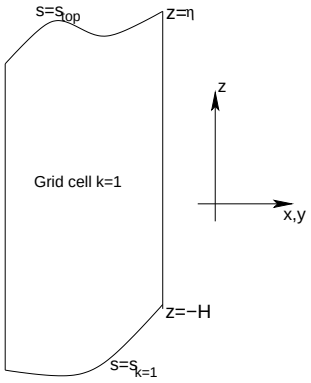

Figure 9. Schematic of an ocean grid cell next to the ocean surface labeled by $k = 1$. Its top face is at $z = \eta$, and the bottom is a surface of constant generalized vertical coordinate $s = s_{k=1}$.

For a grid cell adjacent to the ocean surface (Figure 9), we assume that just the upper face of this cell abuts the boundary between the ocean and the atmosphere or sea ice. The ocean surface is a time dependent boundary with $z = \eta(x, y, t)$. The outward normal $\hat{\mathbf{n}}_\eta$ is given by equation (25), and its area element $\mathrm{d}A_\eta$ is given by equation (26).

As the surface can move, we must measure the advective transport with respect to the moving surface. Just as in the dia-surface transport discussed in Section 2.5, we consider the velocity of a reference point on the surface

$$\mathbf{v}^{\mathrm{ref}} = \mathbf{u}^{\mathrm{ref}} + \hat{\mathbf{z}}\, w^{\mathrm{ref}}. \tag{80}$$

Since $z = \eta$ represents the vertical position of the reference point, the vertical component of the velocity for this point is given by

$$w^{\mathrm{ref}} = (\partial_t + \mathbf{u}^{\mathrm{ref}} \cdot \nabla)\, \eta \tag{81}$$

which then leads to

$$\mathbf{v}^{\mathrm{ref}} \cdot \nabla\, (z - \eta) = \eta_{,t}. \tag{82}$$

Hence, the advective transport leaving the ocean surface is

$$\begin{aligned} \iint_{z=\eta} \mathrm{d}A_{(\hat{\mathbf{n}})}\, \hat{\mathbf{n}} \cdot (\mathbf{v} - \mathbf{v}^{\mathrm{ref}})\, \rho\, C &= \iint_{z=\eta} \mathrm{d}x\, \mathrm{d}y\, (-\eta_{,t} + w - \mathbf{u} \cdot \nabla \eta)\, \rho\, C \\ &= -\iint_{z=\eta} \mathrm{d}x\, \mathrm{d}y\, \rho_{\mathrm{w}}\, q_{\mathrm{w}}\, C, \end{aligned} \tag{83}$$

where the surface kinematic boundary condition (33) was used. The negative sign on the right hand side arises from our convention that $q_{\rm w} > 0$ represents an input of water to the ocean domain. In summary, the tracer flux leaving the ocean free surface is given by

$$\iint\limits_{z=\eta} \mathrm{d}A_{(\hat{\mathbf{n}})}\, \hat{\mathbf{n}} \cdot [(\mathbf{v} - \mathbf{v}^{\rm ref})\, \rho\, C + \mathbf{J}] = \iint\limits_{z=\eta} \mathrm{d}x\, \mathrm{d}y\, (-\rho_{\rm w}\, q_{\rm w}\, C + \nabla\, (z - \eta) \cdot \mathbf{J}). \tag{84}$$

In the above, we formally require the tracer concentration precisely at the ocean surface $z = \eta$. However, as mentioned at the start of Section 2.4, it is actually a fiction that the ocean surface is a smooth mathematical function. Furthermore, seawater properties precisely at the ocean surface, known generally as *skin properties*, are generally not what an ocean model carries as its prognostic variable in its top grid cell. Instead, the model carries a bulk property averaged over roughly the upper few tens of centimeters. The lectures at this school by Professor Ian Robinson discuss these important points in the context of measuring sea surface temperature from a satellite, where the satellite measures the skin temperature, not the *foundational* or bulk temperature carried by large-scale ocean models.

To proceed in formulating the boundary condition for an ocean climate model, whose grid cells we assume to be at least a meter in thickness, we consider there to be a boundary layer model that provides us with the total tracer flux passing through the ocean surface. Developing such a model is a nontrivial problem in air-sea and ice-sea interaction theory and phenomenology. For present purposes, we do not focus on these details, and instead just introduce this flux in the form

$$Q^{(\rm C)} = -\rho_{\rm w}\, q_{\rm w}\, C_{\rm w} + Q^{(\rm C)}_{(\rm turb)} \tag{85}$$

where $C_{\rm w}$ is the tracer concentration in fresh water. The first term represents the advective transport of tracer through the surface with the fresh water (i.e., ice melt, rivers, precipitation, evaporation). The term $Q^{(\rm C)}_{(\rm turb)}$ arises from parameterized turbulence and/or radiative fluxes, such as sensible, latent, shortwave, and longwave heating appropriate for the temperature equation. A positive value for $Q^{(\rm C)}_{(\rm turb)}$ signals tracer leaving the ocean through its surface. In the special case of zero fresh water flux, then

$$\nabla\, (z - \eta) \cdot \mathbf{J} = Q^{(\rm C)}_{(\rm turb)} \qquad \text{if} \quad q_{\rm w} = 0. \tag{86}$$

In general, it is not possible to make this identification. Instead, we must settle for the general expression

$$\iint_{z=\eta} \mathrm{d}A_{(\hat{\mathbf{n}})}\, \hat{\mathbf{n}} \cdot [(\mathbf{v} - \mathbf{v}^{\mathrm{ref}})\, \rho\, C + \mathbf{J}] = \iint_{z=\eta} \mathrm{d}x\, \mathrm{d}y\, (-\rho_{\mathrm{w}}\, q_{\mathrm{w}}\, C_{\mathrm{w}} + Q^{(\mathrm{C})}_{(\mathrm{turb})}). \quad (87)$$

The above results lead to the thickness weighted tracer budget for the ocean surface grid cell

$$\boxed{\begin{aligned} \partial_t\, (\mathrm{d}z\, \rho\, C) = \mathrm{d}z\, \rho\, \mathcal{S}^{(\mathrm{C})} - \nabla_s \cdot [\mathrm{d}z\, \rho\, (\mathbf{u}\, C + \mathbf{F})] \\ + \Big[\rho\, (w^{(s)}\, C + z_{,s}\, \nabla s \cdot \mathbf{F})\Big]_{s=s_{k=1}} \\ + (\rho_{\mathrm{w}}\, q_{\mathrm{w}}\, C_{\mathrm{w}} - Q^{(\mathrm{turb})}_{(\mathrm{C})}), \end{aligned}} \quad (88)$$

and the corresponding mass budget

$$\boxed{\partial_t\, (\mathrm{d}z\, \rho) = \mathrm{d}z\, \rho\, \mathcal{S}^{(\mathrm{M})} - \nabla_s \cdot (\mathrm{d}z\, \rho\, \mathbf{u}) + (\rho\, w^{(s)})_{s=s_{k=1}} + \rho_{\mathrm{w}}\, q_{\mathrm{w}}.} \quad (89)$$

3.6 Surface boundary condition for salt

We close this section by mentioning the free ocean surface boundary condition for salt and other material tracers. Salt is transferred into the ocean with brackish river water and ice melt of nonzero salinity. Yet evaporation and precipitation generally leave the salt content of the ocean unchanged. In these latter cases, the boundary layer tracer flux (85) vanishes

$$Q^{(\mathrm{salt})} = 0. \quad (90)$$

This trivial boundary condition is also appropriate for many other material tracers, such as those encountered with ocean biogeochemical processes. In these cases, the tracer concentration *is not* altered via the passage of tracer across the surface. Instead, it is altered via the transport of fresh water across the ocean free surface which acts to dilute or concentrate the tracer.

The boundary condition (90) is often replaced in ocean models by a *virtual tracer flux* condition, whereby tracer is transferred into the model in lieu of altering the ocean water mass via the transport of fresh water. Virtual tracer flux boundary conditions are required for rigid lid models (Bryan, 1969) that maintain a constant volume and so cannot incorporate surface fresh water fluxes. However, there remain few rigid lid models in use today, and there is no reason to maintain the virtual tracer flux in the more commonly used free surface models. The differences in solution may be minor for many purposes, especially short

integrations (e.g., less than a year). However, the feedbacks related to climate and climate change may be nontrivial. Furthermore, the changes in model formulation are minor once a free surface algorithm has been implemented. Thus, it is prudent and straightforward to jettison the virtual tracer flux in favor of the physically motivated boundary condition (90) (Huang, 1993 and Griffies et al., 2001).

4. Linear momentum budget

The purpose of this section is to formulate the budget for linear momentum over a finite region of the ocean, with specific application to ocean model grid cells. The material here requires many of the same elements as in Section 3, but with added complexity arising from the vector nature of momentum, and the additional considerations of forces from pressure, friction, gravity, and planetary rotation.

4.1 General formulation

The budget of linear momentum for a finite region of fluid is given by the following relation based on Newton's second and third laws

$$\begin{aligned} \partial_t \left(\iiint \mathrm{d}V \, \rho \, \mathbf{v} \right) = & - \iint \mathrm{d}A_{(\hat{\mathbf{n}})} \, [\, \hat{\mathbf{n}} \cdot (\mathbf{v} - \mathbf{v}^{\mathrm{ref}})] \, \rho \, \mathbf{v} \\ & + \iint \mathrm{d}A_{(\hat{\mathbf{n}})} \, (\hat{\mathbf{n}} \cdot \boldsymbol{\tau} - \hat{\mathbf{n}} \, p) \\ & - \iiint \mathrm{d}V \, \rho \, [\, g \, \hat{\mathbf{z}} + (f + \mathcal{M}) \, \hat{\mathbf{z}} \wedge \mathbf{v}]. \end{aligned} \tag{91}$$

The left hand side is the time tendency of the region's linear momentum. The first term on the right hand side is the advective transport of linear momentum across the boundary of the region, with recognition that the region's boundaries are generally moving with velocity $\mathbf{v}^{\mathrm{ref}}$. The second term is the integral of the contact stresses due to friction and pressure. These stresses act on the boundary of the fluid domain. The stress tensor $\boldsymbol{\tau}$ is a symmetric second order tensor that parameterizes subgrid scale transport of momentum. The final term on the right hand side is the volume integral of body forces due to gravity and the Coriolis force.[10] In addition, there is a body force arising from the nonzero curvature of the spherical space. This curvature leads to the advection metric frequency (see equation (4.49) of Griffies, 2004) $\mathcal{M} = v \, \partial_x \ln \mathrm{d}y - u \, \partial_y \ln \mathrm{d}x$. The

[10] The wedge symbol $\wedge$ represents a vector cross product, also commonly written as $\times$. The wedge is typically used in the physics literature, and is preferred here to avoid confusion with the horizontal coordinate x.

advection metric frequency arises since linear momentum is not conserved on the sphere.[11] Hence, the linear momentum budget picks up this extra term that is a function of the chosen lateral coordinates. The advection metric frequency is analogous to, but far smaller than, the Coriolis frequency.

Unlike the case of the tracer and mass balances considered in Section 3, we do not consider momentum sources interior to the fluid domain. Such may be of interest and can be introduced without difficulty. The goal of the remainder of this section is to consider the linear momentum balance for finite grid cells in an ocean model.

4.2 An interior grid cell

At the west side of a grid cell, $\hat{\mathbf{n}} = -\hat{\mathbf{x}}$ whereas $\hat{\mathbf{n}} = \hat{\mathbf{x}}$ on the east side. Hence, the advective transport of linear momentum entering through the west side of the grid cell and that which is leaving through the east side are given by

$$\text{TRANSPORT ENTERING FROM WEST} = \iint_{x=x_1} \mathrm{d}y\, \mathrm{d}s\; z_{,s}\, u\, (\rho\, \mathbf{v}) \tag{92}$$

$$\text{TRANSPORT LEAVING THROUGH EAST} = -\iint_{x=x_2} \mathrm{d}y\, \mathrm{d}s\; z_{,s}\, u\, (\rho\, \mathbf{v}). \tag{93}$$

Similar results hold for momentum crossing the cell boundaries in the north and south directions. Momentum crossing the top and bottom surfaces of an interior cell is given by

$$\text{TRANSPORT ENTERING FROM THE BOTTOM} = \iint_{s=s_2} \mathrm{d}x\, \mathrm{d}y\; w^{(s)}\, (\rho\, \mathbf{v}) \tag{94}$$

$$\text{TRANSPORT LEAVING FROM THE TOP} = -\iint_{s=s_1} \mathrm{d}x\, \mathrm{d}y\; w^{(s)}\, (\rho\, \mathbf{v}). \tag{95}$$

[11] Angular momentum is conserved for frictionless flow on the sphere in the absence of horizontal boundaries (see Section 4.11.2 of Griffies, 2004).

Forces due to the contact stresses at the west and east sides are given by

$$\text{CONTACT FORCE ON WEST SIDE} = -\iint_{x=x_1} \mathrm{d}y\,\mathrm{d}s\; z_{,s}\,(\hat{\mathbf{x}}\cdot\boldsymbol{\tau} - \hat{\mathbf{x}}\,p) \tag{96}$$

$$\text{CONTACT FORCE ON EAST SIDE} = \iint_{x=x_2} \mathrm{d}y\,\mathrm{d}s\; z_{,s}\,(\hat{\mathbf{x}}\cdot\boldsymbol{\tau} - \hat{\mathbf{x}}\,p) \tag{97}$$

with similar results at the north and south sides. At the top of the cell, $\mathrm{d}A_{(\hat{\mathbf{n}})}\,\hat{\mathbf{n}} = \nabla s\,\mathrm{d}x\,\mathrm{d}y$ whereas $\mathrm{d}A_{(\hat{\mathbf{n}})}\,\hat{\mathbf{n}} = -\nabla s\,\mathrm{d}x\,\mathrm{d}y$ at the bottom. Hence,

$$\text{CONTACT FORCE ON CELL TOP} = \iint_{s=s_{k-1}} \mathrm{d}x\,\mathrm{d}y\; z_{,s}\,(\nabla s\cdot\boldsymbol{\tau} - p\,\nabla s) \tag{98}$$

$$\text{CONTACT FORCE ON CELL BOTTOM} = -\iint_{s=s_k} \mathrm{d}y\,\mathrm{d}s\; z_{,s}\,(\nabla s\cdot\boldsymbol{\tau} - p\,\nabla s). \tag{99}$$

Bringing these results together, and taking limit as the time independent horizontal area $\mathrm{d}x\,\mathrm{d}y \to 0$, leads to the thickness weighted budget for the momentum per horizontal area of an interior grid cell

$$\begin{aligned}
\partial_t\,(\mathrm{d}z\,\rho\,\mathbf{v}) = &-\nabla_s\cdot[\,\mathrm{d}z\,\mathbf{u}\,(\rho\,\mathbf{v})] \\
&+ (w^{(s)}\,\rho\,\mathbf{v})_{s=s_k} - (w^{(s)}\,\rho\,\mathbf{v})_{s=s_{k-1}} \\
&+ \partial_x\,[\,\mathrm{d}z\,(\hat{\mathbf{x}}\cdot\boldsymbol{\tau} - \hat{\mathbf{x}}\,p)] \\
&+ \partial_y\,[\,\mathrm{d}z\,(\hat{\mathbf{y}}\cdot\boldsymbol{\tau} - \hat{\mathbf{y}}\,p)] \\
&+ [z_{,s}\,(\nabla s\cdot\boldsymbol{\tau} - p\,\nabla s)]_{s=s_{k-1}} \\
&- [z_{,s}\,(\nabla s\cdot\boldsymbol{\tau} - p\,\nabla s)]_{s=s_k} \\
&- \rho\,\mathrm{d}z\,[\,g\,\hat{\mathbf{z}} + (f+\mathcal{M})\,\hat{\mathbf{z}}\,\wedge\,\mathbf{v}].
\end{aligned} \tag{100}$$

Note that both the time and horizontal partial derivatives are for positions fixed on a constant generalized vertical coordinate surface. Additionally, we have yet to take the hydrostatic approximation, so these equations are written for the three components of the vertical velocity.

The first term on the right hand side of the thickness weighted momentum budget (100) is the convergence of advective momentum fluxes occurring within the layer. We discussed the analogous flux convergence for the tracer and mass budgets in Section 3.3. The second and third terms arise from the transport of momentum across the upper and lower constant s interfaces. The fourth and fifth terms arise from the

horizontal convergence of pressure and viscous stresses. The sixth and seventh terms arise from the frictional and pressure stresses acting on the constant generalized surfaces. These forces provide an interfacial stress between layers of constant s. Note that even in the absence of frictional stresses, interfacial stresses from pressure acting on the generally curved s surface can transmit momentum between vertically stacked layers. The final term arises from the gravitational force, the Coriolis force, and the advective frequency.

4.3 Cell adjacent to the ocean bottom

As for the tracer and mass budgets, we assume zero mass flux through the ocean bottom at $z = -H(x, y)$. However, there is generally a nonzero stress at the bottom due to both the pressure between the fluid and the bottom, and unresolved features in the flow which can correlate or anti-correlate with bottom topographic features (Holloway, 1999). The area integral of the stresses lead to a force on the fluid at the bottom

$$\mathbf{F}_{\text{bottom}} = - \iint_{z=-H} \mathrm{d}x\, \mathrm{d}y\, [\nabla(z+H) \cdot \boldsymbol{\tau} - p\, \nabla(z+H)]. \tag{101}$$

Details of the stress term requires fine scale information that is generally unavailable. For present purposes we assume that some boundary layer model provides information that is schematically written

$$\boldsymbol{\tau}^{\text{bot}} = \nabla(z+H) \cdot \boldsymbol{\tau} \tag{102}$$

where $\boldsymbol{\tau}^{\text{bot}}$ is a vector bottom stress. Taking the limit as the horizontal area vanishes leads to the thickness weighted budget for momentum per horizontal area of a grid cell next to the ocean bottom

$$\begin{aligned} \partial_t\, (\mathrm{d}z\, \rho\, \mathbf{v}) = &- \nabla_s \cdot [\, \mathrm{d}z\, \mathbf{u}\, (\rho\, \mathbf{v})] - (w^{(s)}\, \rho\, \mathbf{v})_{s=s_{kbot-1}} \\ &+ \partial_x\, [\, \mathrm{d}z\, (\hat{\mathbf{x}} \cdot \boldsymbol{\tau} - \hat{\mathbf{x}}\, p)] \\ &+ \partial_y\, [\, \mathrm{d}z\, (\hat{\mathbf{y}} \cdot \boldsymbol{\tau} - \hat{\mathbf{y}}\, p)] \\ &+ [z_{,s}\, (\nabla s \cdot \boldsymbol{\tau} - p\, \nabla s)]_{s=s_{kbot-1}} \\ &- \boldsymbol{\tau}^{\text{bot}} + p_{\text{b}}\, \nabla(z+H) \\ &- \rho\, \mathrm{d}z\, [\, g\, \hat{\mathbf{z}} + (f + \mathcal{M})\, \hat{\mathbf{z}} \wedge \mathbf{v}]. \end{aligned} \tag{103}$$

4.4 Cell adjacent to the ocean surface

There is a nonzero mass and momentum flux through the upper ocean surface at $z = \eta(x, y, t)$, and contact stresses are applied from resolved and unresolved processes involving interactions with the atmosphere and

sea ice. Following the discussion of the tracer budget at the ocean surface in Section 3.5 leads to the expression for the transport of momentum into the ocean due to mass transport at the surface

$$-\iint \mathrm{d}A_{(\hat{\mathbf{n}})}\, \hat{\mathbf{n}} \cdot [(\mathbf{v} - \mathbf{v}^{\mathrm{ref}})\, \rho\, \mathbf{v} = \iint_{z=\eta} \mathrm{d}x\, \mathrm{d}y\, \rho_{\mathrm{w}}\, q_{\mathrm{w}}\, \mathbf{v}. \tag{104}$$

The force arising from the contact stresses at the surface is written

$$\mathbf{F}_{\mathrm{contact}} = \iint_{z=\eta} \mathrm{d}x\, \mathrm{d}y\, [\nabla\,(z-\eta) \cdot \boldsymbol{\tau} - p\, \nabla\,(z-\eta)]. \tag{105}$$

Bringing these results together leads to the force acting at the ocean surface

$$\mathbf{F}_{\mathrm{surface}} = \iint_{z=\eta} \mathrm{d}x\, \mathrm{d}y\, [\nabla\,(z-\eta) \cdot \boldsymbol{\tau} - p\, \nabla\,(z-\eta) + \rho_{\mathrm{w}}\, q_{\mathrm{w}}\, \mathbf{v}]. \tag{106}$$

Details of the various terms in this force are generally unknown. Therefore, just as for the tracer at $z = \eta$ in Section 3.5, we assume that a boundary layer model provides information about the total force, and that this force is written

$$\mathbf{F}_{\mathrm{surface}} = \iint_{z=\eta} \mathrm{d}x\, \mathrm{d}y\, [\boldsymbol{\tau}^{\mathrm{top}} - p_{\mathrm{a}}\, \nabla\,(z-\eta) + \rho_{\mathrm{w}}\, q_{\mathrm{w}}\, \mathbf{v}_{\mathrm{w}}], \tag{107}$$

where $\mathbf{v}_{\mathrm{w}}$ is the velocity of the fresh water. This velocity is typically taken to be equal to the velocity of the ocean currents in the top cells of the ocean model, but such is not necessarily the case when considering the different velocities of, say, river water and precipitation. The stress $\boldsymbol{\tau}^{\mathrm{top}}$ is that arising from the wind, as well as interactions between the ocean and sea ice. Letting the horizontal area vanish leads to the thickness weighted budget for a grid cell next to the ocean surface

$$\begin{aligned}
\partial_t\,(\mathrm{d}z\, \rho\, \mathbf{v}) = &- \nabla_s \cdot [\,\mathrm{d}z\, \mathbf{u}\,(\rho\, \mathbf{v})] + (w^{(s)}\, \rho\, \mathbf{v})_{s=s_{k=1}} \\
&+ \partial_x\, [\,\mathrm{d}z\, (\hat{\mathbf{x}} \cdot \boldsymbol{\tau} - \hat{\mathbf{x}}\, p)] \\
&+ \partial_y\, [\,\mathrm{d}z\, (\hat{\mathbf{y}} \cdot \boldsymbol{\tau} - \hat{\mathbf{y}}\, p)] \\
&- [z_{,s}\, (\nabla s \cdot \boldsymbol{\tau} - p\, \nabla s)]_{s=s_{k=1}} \\
&+ [\,\boldsymbol{\tau}^{\mathrm{top}} - p_{\mathrm{a}}\, \nabla\,(z-\eta) + \rho_{\mathrm{w}}\, q_{\mathrm{w}}\, \mathbf{v}_{\mathrm{w}}] \\
&- \rho\, \mathrm{d}z\, [\, g\, \hat{\mathbf{z}} + (f + \mathcal{M})\, \hat{\mathbf{z}} \wedge \mathbf{v}].
\end{aligned} \tag{108}$$

5. The pressure force

A hydrostatic fluid maintains the balance $p_{,z} = -\rho\, g$. This balance means that the pressure at a point in a hydrostatic fluid is determined by the weight of fluid above this point. This relation is maintained quite well in the ocean on spatial scales larger than roughly 1km. Precisely, when the squared ratio of the vertical to horizontal scales of motion is small, then the hydrostatic approximation is well maintained. In this case, the vertical momentum budget reduces to the hydrostatic balance, in which case vertical acceleration and friction are neglected. If we are interested in explicitly representing such motions as Kelvin-Helmholtz billows and flow within a convective chimney, vertical accelerations are nontrivial and so the non-hydrostatic momentum budget must be used.

The hydrostatic balance greatly affects the algorithms used to numerically solve the equations of motion. The paper by Marshall et al., 1997 highlights these points in the context of developing an algorithm suited for both hydrostatic and non-hydrostatic simulations. However, so far in ocean modelling, no global simulations have been run at resolutions sufficiently refined to require the non-hydrostatic equations. Additionally, many regional and coastal models, even some with resolutions refined smaller than 1km, still maintain the hydrostatic approximation, and thus they must parameterize the unrepresented non-hydrostatic motions.

At a point in the continuum, the horizontal pressure gradient force for the hydrostatic and non-Boussinesq set of equations can be written[12]

$$\boxed{\begin{aligned} \rho^{-1}\, \nabla_z p &= \rho^{-1}\, (\nabla_s - \nabla_s\, z\, \partial_z)\, p \\ &= \rho^{-1}\, \nabla_s\, p + g\, \nabla_s\, z, \\ &= \nabla_s\, (p/\rho + g\, z) - p\, \nabla_s \rho^{-1} \end{aligned}} \tag{109}$$

where the hydrostatic relation $p_{,z} = -\rho\, g$ was used to reach the second equality. The term $p/\rho + g\, z$ is known as the Montgomery potential. For cases where the density term $\nabla_s \rho$ vanishes (such as when s is proportional to density), the pressure gradient force takes the form of a total gradient, and so it has a zero curl thus facilitating the formulation of vorticity budgets.

In general, the difficulty of numerically realizing the pressure gradient force arises when there are contributions from *both* the Montgomery potential and the density gradient terms in equation (109). Naive discretizations result in both terms being large and of opposite sign in

[12] For a Boussinesq fluid, equation (109) is modified by a factor of ρ/ρ_o. Hence, the same issues arise when numerically implementing the pressure gradient force with generalized vertical coordinates in either the Boussinesq or non-Boussinesq fluids.

many regions. Hence, they expose the calculation to nontrivial numerical truncation errors which can lead to spurious pressure gradients that spin up an unforced fluid with initially flat isopycnals. Significant effort has gone into reducing such *pressure gradient errors*, especially in terrain following models where undulations of the coordinate surfaces can be large with realistic bottom topography (e.g., see Figure 12). Some of these issues are summarized, with references, in Section 2 of Griffies et al., 2000a. Perhaps the most promising approach is that proposed by Shchepetkin and McWilliams, 2002. It is notable that difficulties with pressure gradient errors have largely been responsible for the near absence of sigma models being used for long term global ocean climate simulations.[13]

6. Elements of vertical coordinates

As discussed in Griffies et al., 2000a, there are broadly three regimes of the ocean germane to the considerations of a vertical coordinate.

- Upper ocean mixed layer: This is a generally turbulent region dominated by transfers of momentum, heat, freshwater, and tracers with the overlying atmosphere, sea ice, rivers, etc. It is of prime importance for climate system modelling and operational oceanography. It is typically very well mixed in the vertical through three-dimensional convective/turbulent processes. These processes involve non-hydrostatic physics which requires very high horizontal and vertical resolution (i.e., a vertical to horizontal grid aspect ratio near unity) to explicitly represent. A parameterization of these processes is therefore necessary in primitive equation ocean models. In this region, it is essential to employ a vertical coordinate that facilitates the representation and parameterization of these highly turbulent processes. Geopotential and pressure coordinates, or their relatives, are the most commonly used coordinates as they facilitate the use of very refined vertical grid spacing, which can be essential to simulate the strong exchanges between the ocean and atmosphere, rivers, and ice.

- Ocean interior: Tracer transport processes in the ocean interior predominantly occur along neutral directions (McDougall, 1987). The transport is dominated by large scale currents and mesoscale eddy fluctuations. Water mass properties in the interior thus tend

[13]The work of Diansky et al., 2002 is the only case known by the author of a global sigma model used for climate purposes.

to be preserved over large space and time scales (e.g., basin and decade scales). This property of the ocean interior is critical to represent in a numerical simulation of ocean climate. An isopycnal coordinate framework is well suited to this task, whereas geopotential and sigma models have problems associated with numerical truncation errors. As discussed by Griffies et al., 2000b, the problem becomes more egregious as the model resolution is refined, due to the enhanced levels of eddy activity that pumps tracer variance to the grid scale. Quasi-adiabatic dissipation of this variance is difficult to maintain in non-isopycnal models.

- Ocean bottom: The solid earth bottom topography directly influences the overlying currents. In an unstratified ocean, the balanced flow generally follows lines of constant f/H, where f is the Coriolis parameter and H ocean depth. Additionally, there are several regions where density driven currents (overflows) and turbulent bottom boundary layer (BBL) processes act as a strong determinant of water mass characteristics. Many such processes are crucial for the formation of deep water properties in the World Ocean, and for representing coastal processes in regional models. It is for this reason that sigma models have been developed over the past few decades, with their dominant application focused on the coastal and estuarine problem.

These three regimes impact on the design of vertical coordinates for ocean models. In this section, we detail some vertical coordinates and summarize their strengths and weaknesses, keeping in mind the above physical considerations.

6.1 Depth based vertical coordinates

We use depth based vertical coordinates in this section to discretize the Boussinesq equations.[14] Depth based coordinates are also known as *volume based* coordinates, since for a Boussinesq model which uses depth as the vertical coordinate, the volume of interior grid cells is constant in the absence of sources. Correspondingly, depth based coordinates are naturally suited for Boussinesq fluids.

[14]Greatbatch and McDougall, 2003 discuss an algorithm for non-Boussinesq dynamics in a z-model. Their methods are implemented in the MOM4 code of Griffies et al., 2004. This approach may be of special use for non-Boussinesq non-hydrostatic z-models. However, when focusing on hydrostatic models as we do here, pressure based vertical coordinates discussed in Section 6.2 are more convenient.

The equations describing a Boussinesq fluid are derived from the non-Boussinesq set derived in Sections 3 and 4 by replacing all appearances of *in situ* density ρ by a constant density ρ_o, *except* when density is used to compute the buoyancy forces arising from gravity. The density ρ_o is a representative density of the ocean fluid, such as $\rho_o = 1035\,\mathrm{kg\,m^{-3}}$. For much of the ocean, the *in situ* density varies less than 2% from this value (see page 47 of Gill, 1982).

Depth coordinate. With a free surface, the vertical domain over which the z-coordinate $s = z$ ranges is given by the time dependent interval $-H \leq z \leq \eta$. Consequently, the sum of the vertical grid cell increments equals to the total depth of the column $\sum_k \mathrm{d}z = H + \eta$. The trivial specific thickness $z_{,s} = 1$ simplifies the Boussinesq budgets.

The depth coordinate is useful for many purposes in global climate modelling, and models based on depth are the most popular ocean climate models. Their advantages include the following.

- Simple numerical methods have been successfully used in this framework.
- The horizontal pressure gradient can be easily represented in an accurate manner.
- The equation of state for ocean water can be accurately represented in a straightforward manner (e.g., McDougall et al., 2003).
- The upper ocean mixed layer is well parameterized using a z-coordinate.

Unfortunately, these models have some well known disadvantages, which include the following.

- Representation of tracer transport within the quasi-adiabatic interior is cumbersome, with problems becoming more egregious as mesoscale eddies are admitted (Griffies et al., 2000b).
- Representation and parameterization of bottom boundary layer processes and flow are unnatural.

Grid cells have static vertical increments $\mathrm{d}s = \mathrm{d}z$ when $s = z$, except for the top. At the top, $\partial_t(\mathrm{d}z) = \eta_{,t}$. The time dependent vertical range of the coordinate slightly complicates a numerical treatment of the surface cell in z-models (see Griffies et al., 2001 for details of one such treatment). More problematic, however, is the possibility of a vanishing top grid cell. That is, the surface cell can be lost (i.e., can become dry) if the free surface depresses below the depth of the top grid cell's

bottom face. This is a very inconvenient feature that limits the use of z-coordinates.[15] In particular, the following studies may require very refined vertical resolution and/or large undulations of the surface height, and so would not be accessible with a conventional free surface z-model.

- Process studies of surface mixing and biological cycling may warrant very refined upper ocean grid cell thickness, some as refined as 1m.
- Realistic tidal fluctuations in some parts of the World Ocean can reach 10m-20m.
- Coastal models tend to require refined vertical resolution to represent shallow coastal processes along the continental shelves and near-shore.
- When coupled to a sea ice model, the weight of the ice will depress the ocean free surface.

An example of depth coordinates. In some of the following discussion, we illustrate aspects of vertical coordinates by diagnosing values for the coordinates from a realistic z-model run with partial step thicknesses. *Partial steps* have arbitrary thickness which are set to accurately represent the bottom topography. The partial step technology was introduced by Adcroft et al., 1997 in the C-grid MITgcm, and further discussed by Pacanowski and Gnanadesikan, 1998 for the B-grid Modular Ocean Model (MOM). Figure 10 compares the representation of topography in a z-model using partial steps as realized in the MOM code of Griffies et al., 2004. Many z-models have incorporated the partial step technology as it provides an important facility to accurately represent flow and waves near topography.

In the representation of bottom topography, there is an artificial distinction between a vertical face of a cell and its horizontal top and bottom faces. There is no such distinction in the real ocean. As noted in Anne Marie Treguier's lectures at this school, the block structure of topography in z-models has the potential to affect the level of bottom friction. The effects on bottom friction come in by noting that for a C-grid, it is straightforward to run with free-slip side walls as well as bottom faces. In contrast, B-grids use a no-slip side wall and free slip

[15] Linearized free surfaces, in which the budgets for tracer and momentum are formulated assuming a constant top cell thickness, avoid problems with vanishing top cells. However, such models do not conserve total tracer or volume in the presence of a surface fresh water flux (see Griffies et al., 2001, Campin et al., 2004 for discussion).

bottom face. Hence, depending on the interior viscosity and bottom stress parameterization, B-grid models will generally have more bottom friction than C-grid models. With partial steps, the area of the side walls are reduced, thus reducing the area of no-slip side walls in the B-grid. The effective bottom friction in the B-grid is therefore less with partial step topography.

Because of partial steps, the level next to the ocean bottom has grid cell centers that are generally at different depths. That is, the bottom cell in a partial step z-model is likened to a sigma-layer. All other cells, including the surface, have grid cell centers that are at fixed depths. Figure 11 illustrates the lines of constant partial step depth for this model.

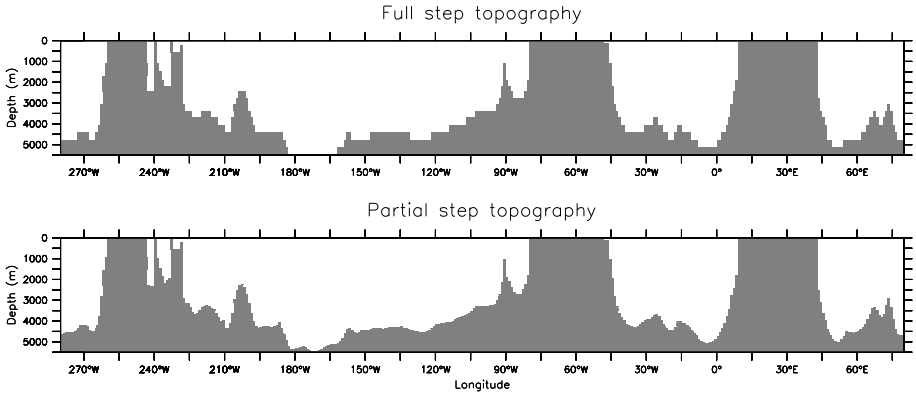

Figure 10. Comparison of the partial step versus full step representation of topography along the equator as realized in the z-model discussed by Griffies et al., 2005. The model horizontal grid has one degree latitudinal resolution. The main differences are in the deep ocean in regions where the topographic slope is gradual. Steep sloped regions, and those in the upper ocean with refined vertical resolution, show less distinctions.

Depth deviation coordinate. The depth deviation coordinate $s = z - \eta$ removes the restriction on upper ocean grid cell resolution present with $s = z$. That is, $s = 0$ is the time independent coordinate value of the ocean surface, no matter how much the free surface depresses or grows. Hence, no surface cells vanish so long as $\eta > -H$. However, $-(H + \eta) \leq s \leq 0$, and so the bottom of a column is a time dependent surface. Consequently, by solving the problem at the ocean surface, the deviation coordinate introduces a problem to the ocean bottom where bottom cells can now vanish.

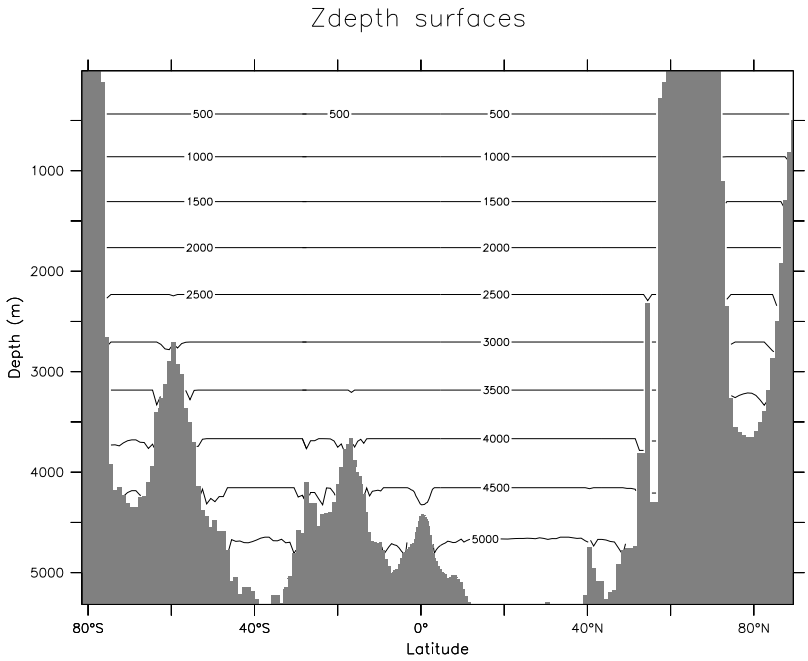

Figure 11. Constant depth surfaces in a realistic ocean model. Deviations from horizontal next to the bottom arise from the use of partial bottom cell thicknesses, as illustrated in Figure 10. Shown here is a section along $150^\circ W$.

Zstar coordinate. To overcome problems with vanishing surface and/or bottom cells, we consider the *zstar* coordinate

$$z^* = H\,(z-\eta)/(H+\eta). \tag{110}$$

This coordinate is closely related to the "eta" coordinate used in many atmospheric models (see Black, 1994 for a review). It was originally used in ocean models by Stacey et al., 1995 for studies of tides next to shelves, and it has been recently promoted by Adcroft and Campin, 2004 for global climate modelling.

The surfaces of constant z^* are quasi-horizontal. Indeed, the z^* coordinate reduces to z when η is zero. In general, when noting the large differences between undulations of the bottom topography versus undulations in the surface height, it is clear that surfaces constant z^* are

very similar to the depth surfaces shown in Figure 11. These properties greatly reduce difficulties of computing the horizontal pressure gradient relative to terrain following sigma models discussed next. Additionally, since $z^* = z$ when $\eta = 0$, no flow is spontaneously generated in an unforced ocean starting from rest, regardless the bottom topography. This behavior is in contrast to the case with sigma models, where pressure gradient errors in the presence of nontrivial topographic variations can generate spontaneous flow from a resting state. The quasi-horizontal nature of the coordinate surfaces also facilitates the implementation of neutral physics parameterizations in z^* models using the same techniques as in z-models (see Chapters 13-16 of Griffies, 2004 for a discussion of neutral physics in z-models).

The range over which z^* varies is time independent $-H \leq z^* \leq 0$. Hence, all cells remain nonvanishing, so long as the surface height maintains $\eta > -H$. This is a minor constraint relative to that encountered on the surface height when using $s = z$ or $s = z - \eta$.

Because z^* has a time independent range, all grid cells have static increments $\mathrm{d}s$, and the sum of the vertical increments yields the time independent ocean depth $\sum_k \mathrm{d}s = H$. The z^* coordinate is therefore invisible to undulations of the free surface, since it moves along with the free surface. This property means that no spurious vertical transport is induced across surfaces of constant z^* by motion of external gravity waves. Such spurious transport can be a problem in z-models, especially those with tidal forcing. Quite generally, the time independent range for the z^* coordinate is a very convenient property that allows for a nearly arbitrary vertical resolution even in the presence of large amplitude fluctuations of the surface height.

Depth sigma coordinate. The depth-sigma coordinate

$$\sigma = (z - \eta)/(H + \eta) \tag{111}$$

is the canonical *terrain following* coordinate. Figure 12 illustrates this coordinate in a realistic model. The sigma coordinate has a long history of use in coastal modelling. For reviews, see Greatbatch and Mellor, 1999 and Ezer et al., 2002. Models based on the sigma coordinate have also been successfully extended to basinwide studies, as well as recent global work by Diansky et al., 2002.

Just as for $z^* = H\,\sigma$, the range over which the sigma coordinate varies is time independent and given by $-1 \leq \sigma \leq 0$. Hence, all cells have static grid increments $\mathrm{d}s$, and the sum of the vertical increments yields unity $\sum_k \mathrm{d}s = 1$. So long as the surface height is not depressed

deeper than the ocean bottom (i.e., so long as $\eta > -H$), then all cells remain nonvanishing.[16]

In addition to not worrying about vanishing grid cells, some key advantages of sigma models are the following.

- They provide a natural framework to represent bottom influenced flow and to parameterize bottom boundary layer processes.
- Thermodynamic effects associated with the equation of state are well represented.

However, some of the disadvantages are the following:

- As with the z-models, the representation of the quasi-adiabatic interior is cumbersome due to numerical truncation errors inducing unphysically large levels of spurious mixing, especially in the presence of vigorous mesoscale eddies. Parameterization of these processes using neutral physics schemes may be more difficult numerically than in the z-models. The reason is that neutral directions generally have slopes less than 1/100 relative to the horizontal, but can have order unity slopes relative to sigma surfaces. The larger relative slopes precludes the *small slope approximation* commonly made with z-model implementations of neutral physics. The small slope approximation provides for simplification of the schemes, and improves computational efficiency.
- Sigma models have difficulty accurately representing the horizontal pressure gradient in the presence of realistic topography, where slopes are commonly larger than 1/100.

Although there are regional simulations using terrain following models, Griffies et al., 2000a notes that there are few examples of global climate models running with this vertical coordinate. Diansky et al., 2002 is the only exception known to the author. This situation is largely due to problems representing realistic topography without incurring unacceptable pressure gradient errors, as well as difficulties implementing parameterizations of neutral physical processes. There are notable efforts to resolve these problems, such as the pressure gradient work of Shchepetkin and McWilliams, 2002. Continued efforts along these lines may soon facilitate the more common use of terrain following coordinates for global ocean climate modelling.

[16] If $\eta < -H$, besides drying up a region of ocean, the specific thickness $z_{,s} = H + \eta$ changes sign, which signals a singularity in the vertical grid definition. The same problem occurs for the z^* coordinate.

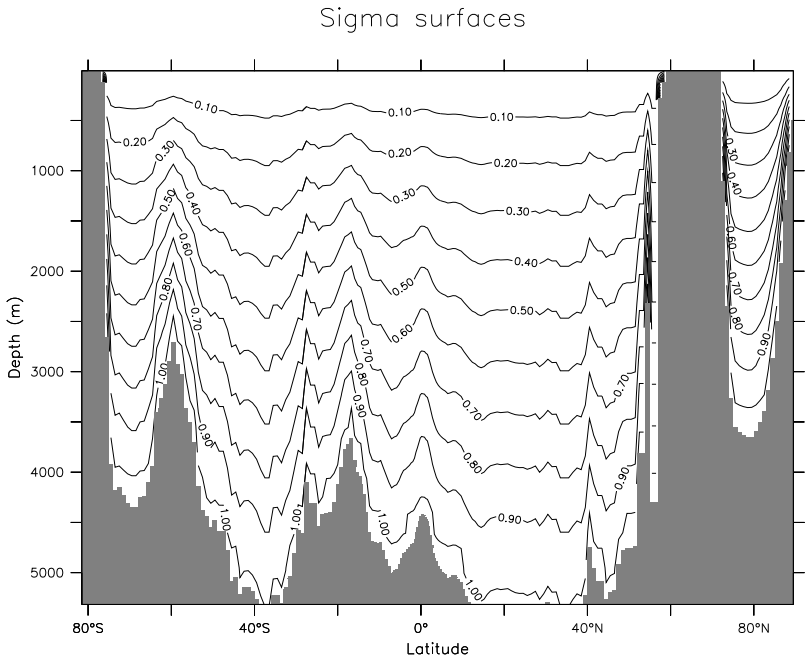

Figure 12. Constant sigma surfaces as diagnosed in a z-model. Shown here is a section along $150^{\circ}W$, as in Figure 11. Note the strong variations in the contours, as determined by changes in the bottom topography.

Summary of the depth based vertical coordinates. Depth based vertical coordinates are naturally used for Boussinesq equations. These coordinates and their specific thicknesses $z_{,s}$ are summarized in Table 2.1. Notably, both the sigma and zstar coordinates have time independent ranges, but time dependent specific thicknesses. In contrast, the depth and depth deviation coordinates have time dependent depth ranges and time independent specific thicknesses. If plotted with the same range as those given in Figure 11, surfaces of constant depth deviation and constant zstar are indistinguishable from surfaces of constant depth. This result follows since the surface height undulations are so much smaller than undulations in the bottom topography, thus making the depth deviation and zstar coordinates very close to horizontal in most parts of the ocean.

Coordinate	**Definition**	**Range**	$z_{,s}$
geopotential	z	$-H \leq z \leq \eta$	1
z-deviation	$z' = z - \eta$	$-(H+\eta) \leq z' \leq 0$	1
z-star	$z^* = H\,(z-\eta)/(H+\eta)$	$-H \leq z^* \leq 0$	$1+\eta/H$
z-sigma	$\sigma = (z-\eta)/(H+\eta)$	$-1 \leq \sigma \leq 0$	$H+\eta$

Table 2.1. Table of vertical coordinates based on depth. These coordinates are naturally used for discretizing the Boussinesq equations.

6.2 Pressure based coordinates

The second class of vertical coordinates that we discuss is based on pressure. Pressure based coordinates provide a straightforward way to generalize Boussinesq depth based models to non-Boussinesq pressure models (Huang et al., 2001, DeSzoeke and Samelson, 2002, Marshall et al., 2003, Losch et al., 2004). The reason is that there is an isomorphism between the Boussinesq equations written in depth based coordinates and non-Boussinesq equations written in pressure based coordinates.

Pressure based vertical coordinates of interest include the following:

$$s = p \qquad \text{pressure} \tag{112}$$

$$s = \left(\frac{p - p_{\rm a}}{p_{\rm b} - p_{\rm a}}\right) \qquad \text{pressure-sigma} \tag{113}$$

$$s = p^o_{\rm b} \left(\frac{p - p_{\rm a}}{p_{\rm b} - p_{\rm a}}\right) \qquad \text{pressure-star.} \tag{114}$$

In these equations, p is the hydrostatic pressure, $p_{\rm a}$ is the pressure applied at the ocean surface from any media above the ocean, such as the atmosphere and sea ice, $p_{\rm b}$ is the hydrostatic pressure at the solid-earth lower boundary, and $p^o_{\rm b}$ is a time independent reference pressure, usually taken to be the bottom pressure in a resting ocean.[17] Since $p_{,z} = -\rho\, g < 0$ is single signed for the hydrostatic fluid, pressure provides a well defined vertical coordinate. Strengths and weaknesses of the corresponding depth based coordinates also hold for the pressure based coordinates, with the main difference being that pressure based models are non-Boussinesq.

A technical reason that the pressure based coordinates considered here are so useful for non-Boussinesq hydrostatic modelling is that $\rho\, z_{,s}$

[17] Note that equation (11.64) of Griffies, 2004 used the time dependent $p_{\rm b}$ rather than the time independent reference pressure $p^o_{\rm b}$. The former vertical coordinate has not been used in practice, and so we focus here on that coordinate defined with the reference pressure $p^o_{\rm b}$.

Coordinate	Definition	Range	$g\,\rho\,z_{,s}$
pressure	p	$p_{\rm a} \le p \le p_{\rm b}$	-1
p-deviation	$p' = p - p_{\rm a}$	$0 \le p' \le p_{\rm b} - p_{\rm a}$	-1
pstar	$p^* = p^o_{\rm b}\,(p - p_{\rm a})/(p_{\rm b} - p_{\rm a})$	$0 \le p^* \le p^o_{\rm b}$	$-(p_{\rm b} - p_{\rm a})/p^o_{\rm b}$
p-sigma	$\sigma = (p - p_{\rm a})/(p_{\rm b} - p_{\rm a})$	$0 \le \sigma \le 1$	$-(p_{\rm b} - p_{\rm a})$

Table 2.2. Table of vertical coordinates based on pressure. These coordinates are naturally used for non-Boussinesq dynamics.

is either a constant or a two-dimensional field. In contrast, for depth based models $\rho\, z_{,s}$ is proportional to the three-dimensional *in situ* density ρ, thus necessitating special algorithmic treatment for non-Boussinesq z-models (see the discussions in Greatbatch and McDougall, 2003 and Griffies, 2004). Table 2.2 summarizes some pressure based coordinates.

As Table 2.2 reveals, the specific thickness $z_{,s}$ is negative for the pressure-based coordinates, whereas it is positive for the depth-based coordinate (Table 2.1). The sign change arises since upward motion in a fluid column increases the geopotential coordinate z yet decreases the hydrostatic pressure p. To establish a convention, we assume that the thickness of a grid cell in z space is always positive

$$\mathrm{d}z = z_{,s}\,\mathrm{d}s > 0 \tag{115}$$

as is the case in the conventional z-models. With $z_{,s} < 0$ for the pressure-based vertical coordinates, the thickness of grid cells in s space is negative

$$\mathrm{d}s < 0 \qquad \text{for pressure-based coordinates with } z_{,s} < 0. \tag{116}$$

6.3 Isopycnal coordinates

Isopycnal models discretize the vertical into potential density classes. Some key advantages of isopycnal models are the following:

- Tracer transport in the ocean interior is well represented due to the natural ability of these models to maintain water mass properties.
- The bottom topography is represented in a piecewise linear fashion, hence avoiding the need to distinguish bottom from side as traditionally done with z-models.
- In some cases, flow near topographically critical regions, such as overflows, can be well resolved by isopycnal models due to the natural tendency of the coordinate surfaces to become refined in these regions.

- For a fluid with a linear equation of state, the horizontal pressure gradient can be easily represented.
- For an adiabatic fluid, the volume (for a Boussinesq fluid) or mass (for a non-Boussinesq fluid) between isopycnals is conserved.

Some of the disadvantages are the following:

- Representing the effects of a realistic (nonlinear) equation of state is cumbersome.
- The thermal wind balance is based on *in situ* density, not potential density. Hence, the further away from the reference pressure, the less accurate the pressure gradient force can be represented solely by the isopycnal gradient of the Montgomery.
- An isopycnal coordinate is inappropriate for regions where density becomes unstratified, such as mixed layers or deep convection regions.

Figure 13 illustrates isopycnal surfaces for a section in the model used to generate Figures 11 and 12.

6.4 Two algorithms

Adcroft and Hallberg, 2004 distinguish two classes of algorithms used to update the model state: quasi-Eulerian and quasi-Lagrangian. The main distinguishing characteristic of these algorithms is how they compute the dia-surface velocity component (Section 2.5). The two algorithm classes have traditionally been associated with two classes of vertical coordinates.

- Quasi-Eulerian algorithms diagnose their vertical velocity component from the *continuity equation*. Geopotential and sigma models have traditionally employed this approach.
- Quasi-Lagrangian algorithms set the vertical velocity component based on specified constraints, and they update the thickness betwen layers via the continuity equation to prognostically move layers around. Isopycnal vertical coordinate models typically use this approach. For example, adiabatic simulations with isopycnal coordinates set the diapycnal velocity component to zero, thus exactly preserving the integrity of the chosen density classes. For non-adiabatic simulations, the diapycnal flux is based on parameterizations of diabatic processes such as arise from the nonlinear equation of state or small scale mixing. A summary of these ideas

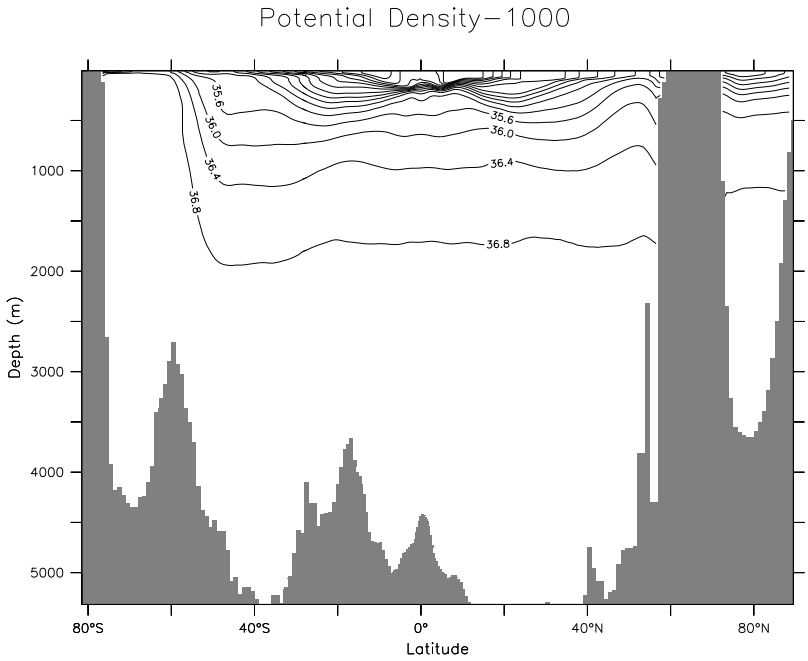

Figure 13. Constant potential density surfaces (minus 1000) in units of $\mathrm{kg\,m^{-3}}$. Potential density is here referenced to 2000db, which is the common reference for isopycnal models based on the work of Sun et al., 1999. Shown here is a section along $150^\circ W$, as in Figure 11. Note the weak stratification in the deep, which is spanned by only one density layer. However, in a realistic isopycnal model, the choice of density classes used to partition the ocean would be non-uniform, in contrast to that used here. In that way, the model will have more layers in the deep and so will better represent interactions with the bottom topography than suggested by this figure.

can be found in Chassignet and Bleck's lectures in this volume, as well as Bleck's lectures in Chassignet and Verron, 1998.

Notably, it is possible to, say, design a z-coordinate model based on quasi-Lagrangian methods, or isopycnal models based on quasi-Eulerian methods. However, such has traditionally not been the case, with the distinctions mentioned above the usual situation.

There is presently no general consensus in the ocean modelling community regarding the best choice of vertical coordinate or the best al-

gorithm methodology. For example, those aiming to faithfully represent the ocean's quasi-adiabatic interior generally prefer an isopycnal layered model using quasi-Lagrangian methods over either terrain following or geopotential models using quasi-Eulerian methods. However, there have been decades of experience with z-models for global climate modelling, largely due to the simplicity of representing and parameterizing air-sea and ice-sea interactions as well as the ocean mixed layer. Hence, these models remain the dominant tool for global climate modelers, even given their well known problems with spurious mixing and difficulties handling overflow processes (see the discussion in Griffies et al., 2000a). Additionally, non-hydrostatic models, such as that from Marshall et al., 1997, have traditionally used geopotential coordinates. Indeed, there is presently no non-hydrostatic algorithm for use in the ocean that is based on a quasi-Lagrangian algorithm. That is, all layered models for the ocean are hydrostatic. Finally, those focusing on shallow ocean dynamics and estuaries have traditionally chosen terrain following coordinates due to their fidelity with bottom boundary layer processes. However, such models have only recently been employed for global climate studies, largely due to difficulties with pressure gradient errors (see Section 2 of Griffies et al., 2000a).

In summary, it is unlikely that modelers will arrive at one universally best vertical coordinate. Instead, vertical coordinates will remain chosen for the particular model application in mind. Modelers may, however, converge on an optimal algorithm methodology, especially if quasi-Lagrangian methods can be extended to non-hydrostatic models. In general, it is useful for model designs to evolve from being based on a single vertical coordinate, to model environments mentioned in Section 1.3 that are flexible enough to include many vertical coordinate algorithms.

7. Closing remarks

It is incumbent on ocean model designers and developers to provide a thorough and pedagogical rationalization of their codes, from the basic equations that the model aims to integrate, to the limitations of their subgrid scale (SGS) parameterizations. Likewise, it is essential that model users understand elements of the model algorithms and SGS parameterizations. The sophisticated and productive use of ocean models comes from a firm understanding of model fundamentals. It is hoped that through more schools such as this one or those documented by O'Brien, 1986, Chassignet and Verron, 1998, and others, as well as books on the subject of geophysical fluid modelling such as Haltiner and

Williams, 1980, Durran, 1999, Haidvogel and Beckmann, 1999, Kantha and Clayson, 2000a, Kantha and Clayson, 2000b, and Griffies, 2004, students aiming to use ocean models will readily learn to scrutinize the simulation's output in a scientifically sound and rational manner so as to improve the models, and ultimately to better understand and predict the ocean.

Acknowledgments

These lectures were prepared for the GODAE Summer School on Operational Oceanography held at La Londe Les Maures, France from September 20 to October 1, 2004. I thank the organizers Eric Chassignet and Jacques Verron for inviting me to give these lectures, and for developing a fine program in a wonderful place. Many students provided important feedback to help develop these lectures, as did Anne Marie Treguier. I also thank Alistair Adcroft, Bob Hallberg, and Trevor McDougall for their lessons over the years about generalized vertical coordinates.

References

Adcroft, A. and Hallberg, R. W. (2004). On methods for solving the oceanic equations of motion in generalized vertical coordinates. *Ocean Modelling*, page in press.

Adcroft, A., Hill, C., and Marshall, J. (1997). Representation of topography by shaved cells in a height coordinate ocean model. *Monthly Weather Review*, 125:2293–2315.

Adcroft, A., Hill, C., and Marshall, J. (1999). A new treatment of the coriolis terms in c-grid models at both high and low resolutions. *Monthly Weather Review*, 127:1928–1936.

Adcroft, Alistair and Campin, Jean-Michel (2004). Rescaled height coordinates for accurate representation of free-surface flows in ocean circulation models. *Ocean Modelling*, 7:269–284.

Arakawa, Akio and Lamb, Vivian R. (1977). The UCLA general circulation model. In Chang, Julius, editor, *Methods in Computational Physics: General Circulation Models of the Atmosphere*, volume 17, pages 174–265. Academic Press.

Black, Thomas L. (1994). The new NMC mesoscale eta model: description and forecast examples. *Weather and Forecasting*, 9:265–278.

Blayo, Eric and Debreu, L. (1999). Adaptive mesh refinement for finite difference ocean model: some first experiments. *Journal of Physical Oceanography*, 29:1239–1250.

Bleck, Rainer (2002). An oceanic general circulation model frame in hybrid isopycnic-cartesian coordinates. *Ocean Modelling*, 4:55–88.

Bryan, K. (1969). A numerical method for the study of the circulation of the world ocean. *Journal of Computational Physics*, 4:347–376.

Campin, Jean-Michel, Adcroft, Alistair, Hill, Chris, and Marshall, John (2004). Conservation of properties in a free-surface model. *Ocean Modelling*, 6:221–244.

Chassignet, Eric P. and Verron, J. (1998). *Ocean Modeling and Parameterization*, volume 516 of *NATO ASI Mathematical and Physical Sciences Series*. Kluwer Academic Publishers.

DeSzoeke, R. A. and Samelson, R. M. (2002). The duality between the Boussinesq and non-Boussinesq hydrostatic equations of motion. *Journal of Physical Oceanography*, 32:2194–2203.

Diansky, N.A., Bagno, A.V., and Zalensy, V.B. (2002). Global ocean circulation sigma-model and its sensitivity to the wind stress forcing. *Izvestia, Atmospheric and Oceanic Physics*, 38:477–494.

Durran, D. R. (1999). *Numerical Methods for Wave Equations in Geophysical Fluid Dynamics*. Springer Verlag, Berlin. 470 pp.

Ezer, T., Arango, H., and Shchepetkin, A. F. (2002). Developments in terrain-following ocean models: Intercomparisons of numerical aspects. *Ocean Modelling*, 4:249–267.

Gill, A. (1982). *Atmosphere-Ocean Dynamics*, volume 30 of *International Geophysics Series*. Academic Press, London. 662 + xv pp.

Greatbatch, R. J. and McDougall, Trevor J. (2003). The non-Boussinesq temporal-residual-mean. *Journal of Physical Oceanography*, 33:1231–1239.

Greatbatch, Richard J. and Mellor, G. L. (1999). An overview of coastal ocean models. In Mooers, C.N.K., editor, *Coastal Ocean Prediction*, volume 56 of *Coastal and Estuarine Studies*, pages 31–57. American Geophysical Union.

Griffies, Stephen M. (2004). *Fundamentals of ocean climate models*. Princeton University Press, Princeton, USA. 496 pages.

Griffies, Stephen M., Böning, C., Bryan, F. O., Chassignet, E. P., Gerdes, R., Hasumi, H., Hirst, A., Treguier, A.-M., and Webb, D. (2000a). Developments in ocean climate modelling. *Ocean Modelling*, 2:123–192.

Griffies, Stephen M. Gnanadesikan, Anand, Dixon, Keith W. Dunne, John P. Gerdes, Rüdiger, Harrison, Matthew J. Held, Isaac M. Pacanowski, Ronald C. Rosati, Anthony, Samuels, Bonita L. Spelman, Michael J. Winton, Michael, and Zhang, Rong (2005). Formulation of an ocean model for use in global climate simulations. *Ocean Modelling*, page in prep.

Griffies, Stephen M., Harrison, Matthew J., Pacanowski, Ronald C., and Rosati, Anthony (2004). *A Technical Guide to MOM4*. NOAA/Geophysical Fluid Dynamics Laboratory, Princeton, USA. 337 pp.

Griffies, Stephen M., Pacanowski, R. C., and Hallberg, Robert W. (2000b). Spurious diapycnal mixing associated with advection in a z-coordinate ocean model. *Monthly Weather Review*, 128:538–564.

Griffies, Stephen M., Pacanowski, R. C., Schmidt, R. M., and Balaji, V. (2001). Tracer conservation with an explicit free surface method for z-coordinate ocean models. *Monthly Weather Review*, 129:1081–1098.

Haidvogel, D. B. and Beckmann, A. (1999). *Numerical Ocean Circulation Modeling*. Imperial College Press, London.

Hallberg, Robert W. (1997). Stable split time stepping schemes for large-scale ocean modeling. *Journal of Computational Physics*, 135:54–65.

Haltiner, G. T. and Williams, R. T. (1980). *Numerical Prediction and Dynamic Meteorology*. John Wiley and Sons, New York, USA.

Holloway, Greg (1999). Moments of probable seas: statistical dynamics of Planet Ocean. *Physica D*, 133:199–214.

Huang, R. X. (1993). Real freshwater flux as a natural boundary condition for the salinity balance and thermohaline circulation forced by evaporation and precipitation. *Journal of Physical Oceanography*, 23:2428–2446.

Huang, R. X., Jin, Xiangze, and Zhang, Xuehong (2001). An oceanic general circulation model in pressure coordinates. *Advances in Atmospheric Physics*, 18:1–22.

Jackett, D. R., McDougall, T. J., Feistel, R., Wright, D. G., and Griffies, Stephen M. (2004). Updated algorithms for density, potential temperature, conservative temperature, and freezing temperature of seawater. *Journal of Atmospheric and Oceanic Technology*, page submitted.

Kantha, L. H. and Clayson, C. A. (2000a). *Numerical Models of Oceans and Oceanic Processes*. Academic Press, New York, USA. 936 pp.

Kantha, L. H. and Clayson, C. A. (2000b). *Small Scale Processes in Geophysical Fluid Flows*. Academic Press, New York, USA. 883 pp.

Losch, M., Adcroft, A., and Campin, J.-M. (2004). How sensitive are coarse general circulation models to fundamental approximations in the equations of motion? *Journal of Physical Oceanography*, 34:306–319.

Madec, G. and Imbard, M. (1996). A global ocean mesh to overcome the North Pole singularity. *CD*, 12:381–388.

Marshall, J., Adcroft, A., Campin, J.-M., and Hill, C. (2003). Atmosphere-ocean modeling exploiting fluid isomorphisms. *Journal of Physical Oceanography*. in press.

Marshall, J., Hill, C., Perelman, L., and Adcroft, A. (1997). Hydrostatic, quasi-hydrostatic, and nonhydrostatic ocean modeling. *Journal of Geophysical Research*, 102:5733–5752.

McDougall, T. J. (1987). Neutral surfaces. *Journal of Physical Oceanography*, 17:1950–1967.

McDougall, T. J. (1995). The influence of ocean mixing on the absolute velocity vector. *Journal of Physical Oceanography*, 25:705–725.

McDougall, T. J. (2003). Potential enthalpy: a conservative oceanic variable for evaluating heat content and heat fluxes. *Journal of Physical Oceanography*, 33:945–963.

McDougall, T. J., Jackett, D. R., Wright, D. G., and Feistel, R. (2003). Accurate and computationally efficient algorithms for potential temperature and density of seawater. *Journal of Atmospheric and Oceanic Technology*, 20:730–741.

Murray, R. J. (1996). Explicit generation of orthogonal grids for ocean models. *Journal of Computational Physics*, 126:251–273.

O'Brien, James J. (1986). *Advanced Physical Oceanographic Numerical Modelling*. D. Reidel Publishing Company.

Pacanowski, Ronald C. and Gnanadesikan, A. (1998). Transient response in a z-level ocean model that resolves topography with partial-cells. *Monthly Weather Review*, 126:3248–3270.

Shchepetkin, A.F. and McWilliams, J.C. (2002). A method for computing horizontal pressure-gradient force in an ocean model with a non-aligned vertical coordinate. *Journal of Geophysical Research*, 108:35.1–35.34.

Stacey, Michael W., Pond, Stephen, and Nowak, Zenon P. (1995). A numerical model of the circulation in Knight Inlet, British Columbia, Canada. *Journal of Physical Oceanography*, 25:1037–1062.

Sun, S., Bleck, R., Rooth, C., Dukowicz, J., Chassignet, E., and Killworth, P. D. (1999). Inclusion of thermobaricity in isopycnic-coordinate ocean models. *Journal of Physical Oceanography*, 29:2719–2729.

Thuburn, John and Haine, Thomas W.N. (2001). Adjoints of nonoscillatory advection schemes. *Journal of Computational Physics*, 171:616–631.